Proton, helium, and electron spectra during the large solar particle events of October–November 2003

R. A. Mewaldt,[1] C. M. S. Cohen,[1] A. W. Labrador,[1] R. A. Leske,[1] G. M. Mason,[2,3] M. I. Desai,[2] M. D. Looper,[4] J. E. Mazur,[4] R. S. Selesnick,[4] and D. K. Haggerty[5]

Received 1 February 2005; revised 1 June 2005; accepted 24 June 2005; published 30 September 2005.

[1] The extraordinary period from late October through early November 2003 was marked by more than 40 coronal mass ejections (CME), eight X-class flares, and five large solar energetic particle (SEP) events. Using data from instruments on the ACE, SAMPEX, and GOES-11 spacecraft, the fluences of H, He, O, and electrons have been measured in these five events over the energy interval from ~0.1 to >100 MeV/nucleon for the ions and ~0.04 to 8 MeV for electrons. The H, He, and O spectra are found to resemble double power laws, with a break in the spectral index between ~5 and ~50 MeV/nucleon which appears to depend on the charge-to-mass ratio of the species. Possible interpretations of the relative location of the H and He breaks are discussed. The electron spectra can also be characterized by double power laws, but incomplete energy coverage prevents an exact determination of where and how the spectra steepen. The proton and electron fluences in the 28 October 2003 SEP event are comparable to the largest observed during the previous solar maximum, and within a factor of 2 or 3 of the largest SEP events observed during the last 50 years. The 2-week period covered by these observations accounted for ~20% of the high-energy solar-particle fluence over the years from 1997 to 2003. By integrating over the energy spectra, the total energy content of energetic protons, He, and electrons in the interplanetary medium can be estimated. After correcting for the location of the events, it is found that the kinetic energy in energetic particles amounts to a significant fraction of the estimated CME kinetic energy, implying that shock acceleration must be relatively efficient in these events.

Citation: Mewaldt, R. A., C. M. S. Cohen, A. W. Labrador, R. A. Leske, G. M. Mason, M. I. Desai, M. D. Looper, J. E. Mazur, R. S. Selesnick, and D. K. Haggerty (2005), Proton, helium, and electron spectra during the large solar particle events of October–November 2003, *J. Geophys. Res.*, *110*, A09S18, doi:10.1029/2005JA011038.

1. Introduction

[2] The 2-week period spanning the last week of October 2003 and the first week of November was marked by some of the most intense solar activity in the history of the space age, including 43 coronal mass ejections (CMEs) [see *Gopalswamy et al.*, 2005], eight X-class flares, some of the largest solar particle events of this solar cycle, and two of the largest geomagnetic storms in history. Figure 1 summarizes measured solar particle intensities of protons and electrons in several energy intervals. Five large solar energetic particle (SEP) events are evident, each associated with an X-class flare and a very fast CME. In the first four of these events the interplanetary shock was still accelerating particles to MeV energies when the shock reached 1 AU. In addition, shocks associated with a number of other CMEs were observed during this period (see http://www.ssg.sr.unh.edu/mag/ace/ACElists/obs_list.html). These five events were also marked by increases in the electron intensity at 1 AU, as shown in the top panel of Figure 1. Electron increases were also observed in association with several of the interplanetary shocks. Table 1 summarizes key properties of the five large SEP events, which, for convenience, are sometimes referred to here by number as events 1 to 5.

[3] The two largest of the solar particle events occurred on consecutive days, following an X17 flare on 28 October 2003 and X10 event on 29 October, both located near central meridian. Both events were associated with very fast CMEs, and in each case the interplanetary shocks driven by the CMEs reached Earth within only ~19 hours. Upon arrival at 1 AU both shocks were still accelerating protons up to energies >15 MeV (see Figure 1).

[4] The events of solar cycle 23 have been the best studied in history as a result of new instrumentation on spacecraft that include ACE, RHESSI, SAMPEX, SOHO, TRACE, Ulysses, and Wind. Many of the solar particle results have focused on new heavy ion measurements,

[1]Physics Department, California Institute of Technology, Pasadena, California, USA.
[2]Department of Physics, University of Maryland, College Park, Maryland, USA.
[3]Also at Institute for Physical Science and Technology, University of Maryland, College Park, Maryland, USA.
[4]The Aerospace Corporation, Los Angeles, California, USA.
[5]Johns Hopkins University Applied Physics Laboratory, Laurel, Maryland, USA.

0148-0227/05/2005JA011038$09.00

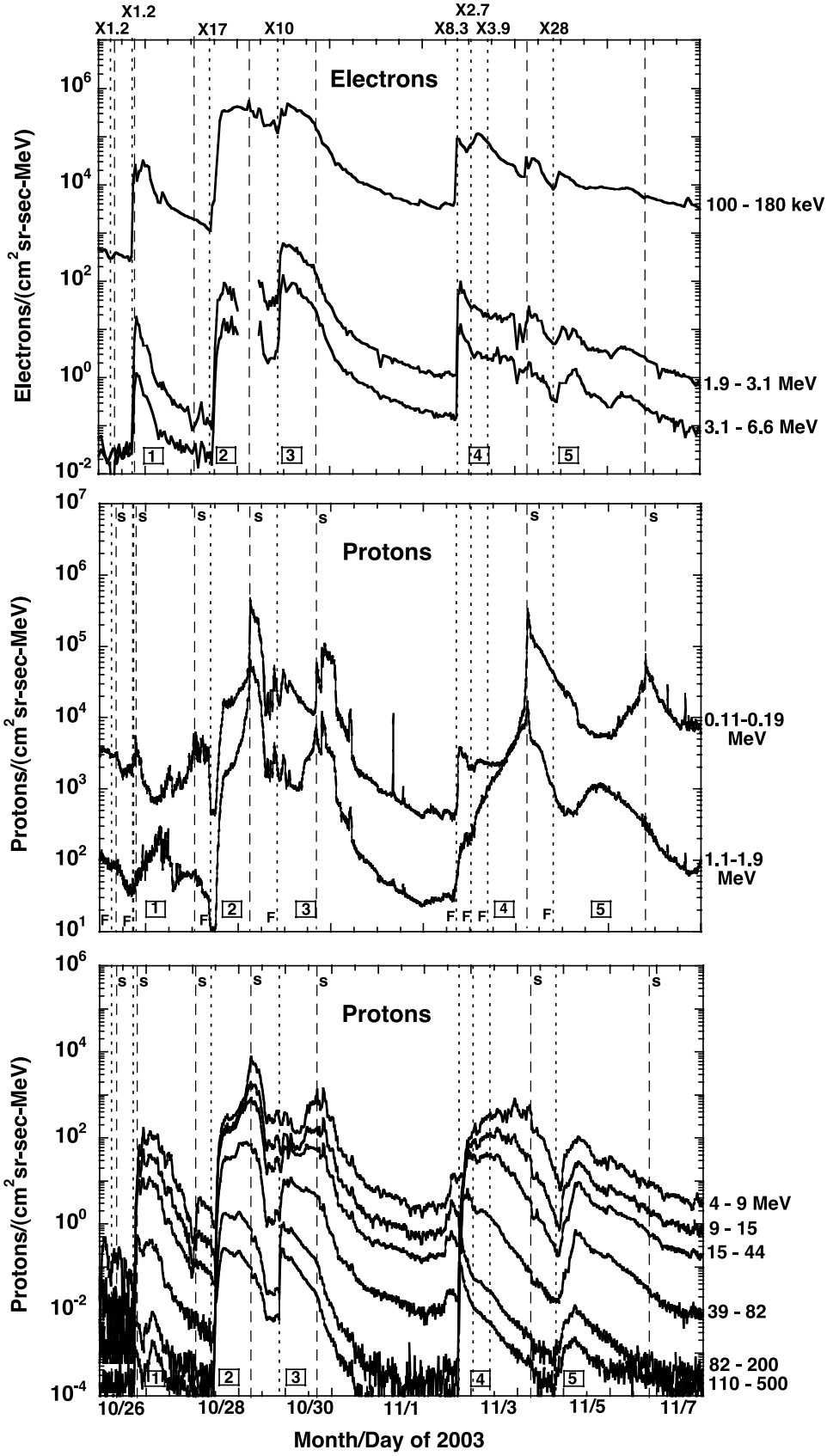
X1.2
X1.2
X17
X10
X2.7
X8.3
X3.9
X28
Electrons
Electrons/(cm2sr-sec-MeV)
100 - 180 keV
1.9 - 3.1 MeV
3.1 - 6.6 MeV
Protons
Protons/(cm2sr-sec-MeV)
0.11-0.19 MeV
1.1-1.9 MeV
Protons
Protons/(cm2sr-sec-MeV)
4 - 9 MeV
9 - 15
15 - 44
39 - 82
82 - 200
110 - 500
10/26
10/28
10/30
11/1
11/3
11/5
11/7
Month/Day of 2003

Figure 1

Table 1. Large Solar Proton Events During October–November 2003

Event	Flare Start Time,[a] UT	GOES X-Ray Flux[a]	Flare Location[a]	CME Velocity[b], km/s	Peak >10 MeV Proton Intensity,[c] $(cm^2\ sr\ s\ MeV)^{-1}$	Shock Time,[d] UT
1	26 Oct 1721	X1.2	N02W38	1537	373	28 Oct 0131
2	28 Oct 0951	X17.2	S16E08	2459	25242	29 Oct 0558
3	29 Oct 2037	X10	S15W02	2029	2158	30 Oct 1619
4	2 Nov 1703	X8.3	S14W56	2598	1356	4 Nov 0559
5	4 Nov 1929	X28	S19W83	2657	303	6 Nov 1919

[a]All flare data are from http://www.sec.noaa.gov/Data/index.html.
[b]From *Gopalswamy et al.* [2005].
[c]Based on the maximum 1-hour average value from GOES-11.
[d]Obtained from http://www-ssg.sr.unh.edu/mag/ace/ACElists/obs_list.html.

obtained for the first time with excellent resolution, statistical accuracy, and energy coverage [e.g., *Cohen et al.*, 2005]. In order to complement these heavy ion data, we have made a concentrated effort to compile data for the most abundant species, H, He, and electrons, species that are often not well measured in instruments that are designed to extend to the iron group.

[5] In this paper we report new observations of the energy spectra of H, He, O, and electrons, integrated over each of the five largest SEP events during October and November 2003. These fluence spectra make use of data from five instruments on three separate spacecraft, the Advanced Composition Explorer (ACE), the Solar, Anomalous, and Magnetospheric Particle Explorer (SAMPEX), and NOAA's 11th Geosynchronous, Operational, Environmental Satellite (GOES-11). These five instruments make it possible to cover the energy interval from ~0.1 MeV/nuc to several hundred MeV/nuc for H, 0.1 to ~80 MeV/nuc for He and O, and ~0.04 to 8 MeV for electrons.

2. Instrumentation

[6] The observations reported here were drawn from the Ultra-Low Energy Isotope Spectrometer (ULEIS), Solar Isotope Spectrometer (SIS), and Electron, Proton, and Alpha Monitor (EPAM) on ACE, the Proton Electron Telescope (PET) on SAMPEX, and the Energetic Particle Sensor (EPS) ion GOES-11. Table 2 summarizes the energy ranges over which H, He, O, and electron data were obtained. In this section we summarize briefly key features of the instruments and their location; additional details about the instruments and about corrections to the data can be found in Appendix A.

[7] The ACE spacecraft, in orbit about the inner Lagrangian point (L1), has its spin axis generally pointed within ~10° of the Sun [*Stone et al.*, 1998a]. The ULEIS [*Mason et al.*, 1998] and SIS [*Stone et al.*, 1998b] instruments are mounted at 60° and 25° to the spin axis, such that they scan the sunward hemisphere as the spacecraft spins, including the nominal ~45° (Parker spiral) angle of the average interplanetary magnetic field. The EPAM instrument on ACE has several telescopes with multiple look directions (see Appendix A and *Gold et al.* [1998]); in this study we use EPAM electron measurements from the LEMS30 telescope mounted at 30° to the spin axis and proton data from the LEMS120 telescope, mounted at 120° from the spin axis and looking in the hemisphere away from the Sun. The LEMS120 telescope was used for proton measurements instead of the LEMS30 telescope as a result of elevated background in the LEMS30 proton channels during this time period [*Haggerty et al.*, 2005].

[8] The Proton-Electron Telescope [*Cook et al.*, 1993] is carried on SAMPEX in a ~600-km near-polar orbit. SAMPEX observes interplanetary particles directly only when over the polar caps. To avoid contamination from Earth's trapped radiation, the data presented here are restricted to times when SAMPEX was above 70° invariant latitude for ions and above 75° for electrons. In addition, a cut was made to include only data taken when the PET telescope was pointed upward, within 40 degrees of the local geomagnetic field direction.

[9] Proton data from ~5 to 200 MeV and He data from 1.3 to 125 MeV/nucleon were obtained from NOAA's GOES-11 satellite which is at geosynchronous altitude (≈6.6 Earth radii). Proton data from the Energetic Particle Sensors (EPS) on the GOES satellites [*Onsager et al.*, 1996] are available from http://spidr2.ngdc.noaa.gov/spidr/in the form of "corrected integral intensities" (>1, >5, >10, >30, >50, >60, and >100 MeV) and also as "corrected differential intensities" (eight energy intervals ranging from 0.8–4.2 MeV up to 200–500 MeV in the case of GOES-11). This study includes data from both of these data sets. Additional differential points were obtained by calculating differences between the hourly average integral points (e.g., the difference between the >5 and >10 MeV intensities results in a differential intensity of 5 to 10 MeV protons). This procedure was also used by *Tylka et al.* [2005] to obtain SEP proton spectra. The results of this differencing technique are in good agreement with the corrected differential intensities, and we have plotted both sets of mea-

Figure 1. Time history of energetic protons and electrons during the period from 26 October 2003 to 7 November 2003. The top panel shows electron data from EPAM/ACE (top trace) and PET/SAMPEX (1.9 to 6.6 MeV). The SAMPEX points are averaged over separate polar passes, including only data obtained at invariant latitudes >75°. It is possible that the intensities shown near the end of 29 October through 30 October (SEP event 3) are overestimated because of background contributions as discussed in section 3.4. The middle panel shows low-energy proton data from ACE/EPAM and the bottom panel includes protons measured by GOES-11 in six different energy intervals. The occurrence of X-class flares (obtained from NOAA) are indicated by dotted vertical lines with the intensity labeled above each line. Interplanetary shocks are indicated by dashed vertical lines labeled by an "s." Major proton events during this interval are labeled 1 to 5.

Table 2. Instruments and Energy Coverage

		Energy Range, MeV or MeV/nucleon			
Instrument	Spacecraft	Protons	Helium	Oxygen	Electrons
ULEIS	ACE	0.16–7.2	0.11–7.2	0.04–9.7	
EPAM	ACE	0.047–4.8			0.038–0.32
SIS	ACE		3.4–29.4	7.0–90	
PET	SAMPEX	19–400	20–80		1.2–8
EPS	GOES-11	4–200	1.3–125		

surements (realizing that they are not independent). We have not used <5 MeV GOES proton or He data because of the greater possibility of geomagnetic influence on the intensities.

3. Observations

3.1. Selection of Time Periods

[10] For the high-energy data from SIS and GOES, the fluences were computed using hourly average intensities, starting with the first hour in which an increase above the preexisting particle background was observed and ending once the event had decayed to an extent that the integrated fluence was no longer increasing, or in some cases, when the next event began. The time intervals when the shock reached 1 AU were included. For PET, we included all polar passes that occurred within the time intervals established using GOES and SIS data. Table 3 includes the time intervals used for the high-energy fluences. These intervals are essentially the same as those used by *Cohen et al.* [2005] except for event 1, where we used a somewhat longer time interval.

[11] In most studies of SEP spectra, the fluences are computed for all energies over a single time interval. However, the extension of spectra to very low energies in the current study makes it necessary to take account of the fact that low-energy particles may arrive significantly later than higher-energy particles. Thus when a new event is observed at high energies, particles near the lower end of our spectra (~0.1 MeV/nuc) may not arrive for another 12 hours or more. Picking a single time interval can thus result in the mixing of particles from more than one event. To avoid this, the start and stop times for the ULEIS and EPAM fluence calculations were adjusted to begin later than for higher energies. The high-energy onset used is the same as that used for SIS and PET, while at lower energies later onset times are chosen which increase as the inverse of the particle speed. Since most of the fluence arrives during the times of peak intensity, the details of these variable onset times do not have a significant effect on the reported fluences.

3.2. Integrated Fluence Spectra of Ions

[12] These five events originated over a wide longitude range, and their associated interplanetary shocks are not all equally proficient at accelerating particles. As a result, the relative contributions of particles accelerated close to the Sun and those accelerated locally depend on energy and vary from event to event, as can be seen from inspection of Figure 1. Only events 1 and 4 are well-connected to Earth and in both cases there is an initial impulsive spike at high energies, arriving soon after the X-ray onset and the launch of the associated CME (see Table 1). The time of maximum of lower-energy (<15 MeV) particles occurs significantly later, suggesting that these particles were trapped by the shock and leaked out gradually as the shock approaches. This is especially evident in the 1–2 MeV profile of event 4, which rises steadily over 2 days until the shock arrives. Once the associated shock does arrive on 4 November, protons are being accelerated only up to energies <10 MeV. In these two events particles accelerated in the inner heliosphere dominate the fluences >10 MeV, and locally accelerated particles contribute significantly only below a few MeV.

[13] Events 2 and 3 originate near central meridian, and as a result particles accelerated at the nose of the shock are initially not well-connected to Earth. It is likely that early in these events much of the fluence comes from the western flank of the shock as it crosses field lines connected to Earth. At lower energies (<40 MeV) the proton intensities continue to rise as the shock approaches and the fluences below ~40 MeV in these events are dominated by the recent history of the shock as it approaches Earth.

[14] The fluences in event 5, which originated at W83, are likely due mainly to the eastern flank of the shock. At energies >4 MeV the intensity maximum is about 10–12 hours after the onset of the event, and locally accelerated particles make significant contributions to the event only below 1 MeV.

[15] The integrated fluence spectra of H, He, and O from these events are shown in Figure 2, plotted as a function of energy/nucleon. Note that all of the spectra have a power law component at energies <1 MeV/nuc, with significant steepening in the energy range from ~10 to 50 MeV/nucleon. In some cases there are also differences in shape between the H, He, and O spectra. In those cases where there is sufficient data available at high energies, including all of the proton spectra, it appears that the high-energy

Table 3. Fluence Measurement Intervals

Event	Flare Date	Onset Time	High-Energy SEP Start	High-Energy SEP End
1	10/26/03	1721	1800 on 10/26	1000 on 10/28
2	10/28/03	1100	1100 on 10/28	2000 on 10/29
3	10/29/03	2037	2100 on 10/29	2400 on 10/31
4	11/2/03	1703	1700 on 11/2	2000 on 11/4
5	11/4/03	1929	2100 on 11/4	1200 on 11/7

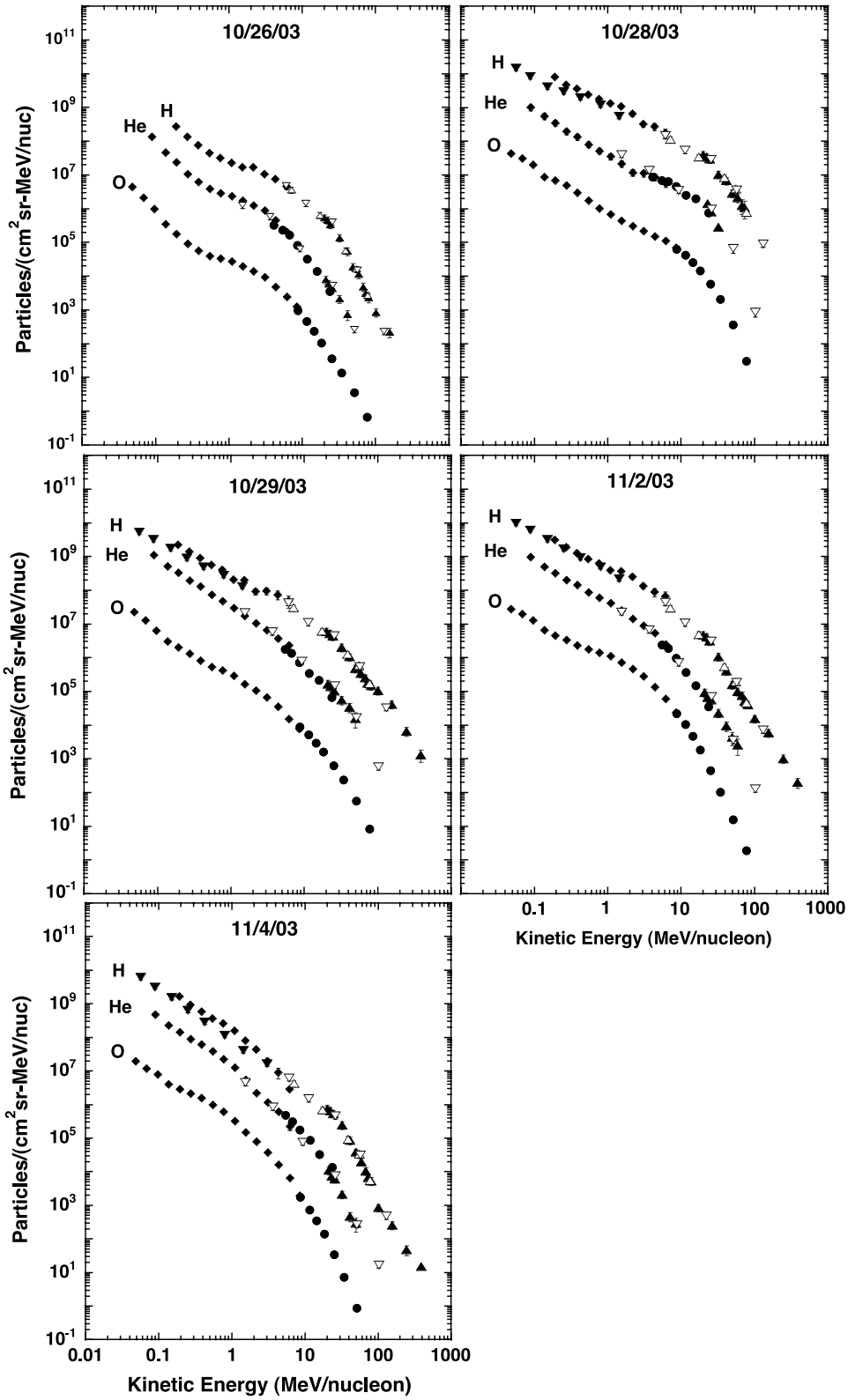

Figure 2. Integrated fluence spectra of H, He, and O for the five SEP events in this study. The data are from ULEIS (filled diamonds), EPAM (downward filled triangles), SIS (filled circles), PET (filled upward triangles), and GOES-11 (upward and downward open triangles). See color version of this figure at back of this issue.

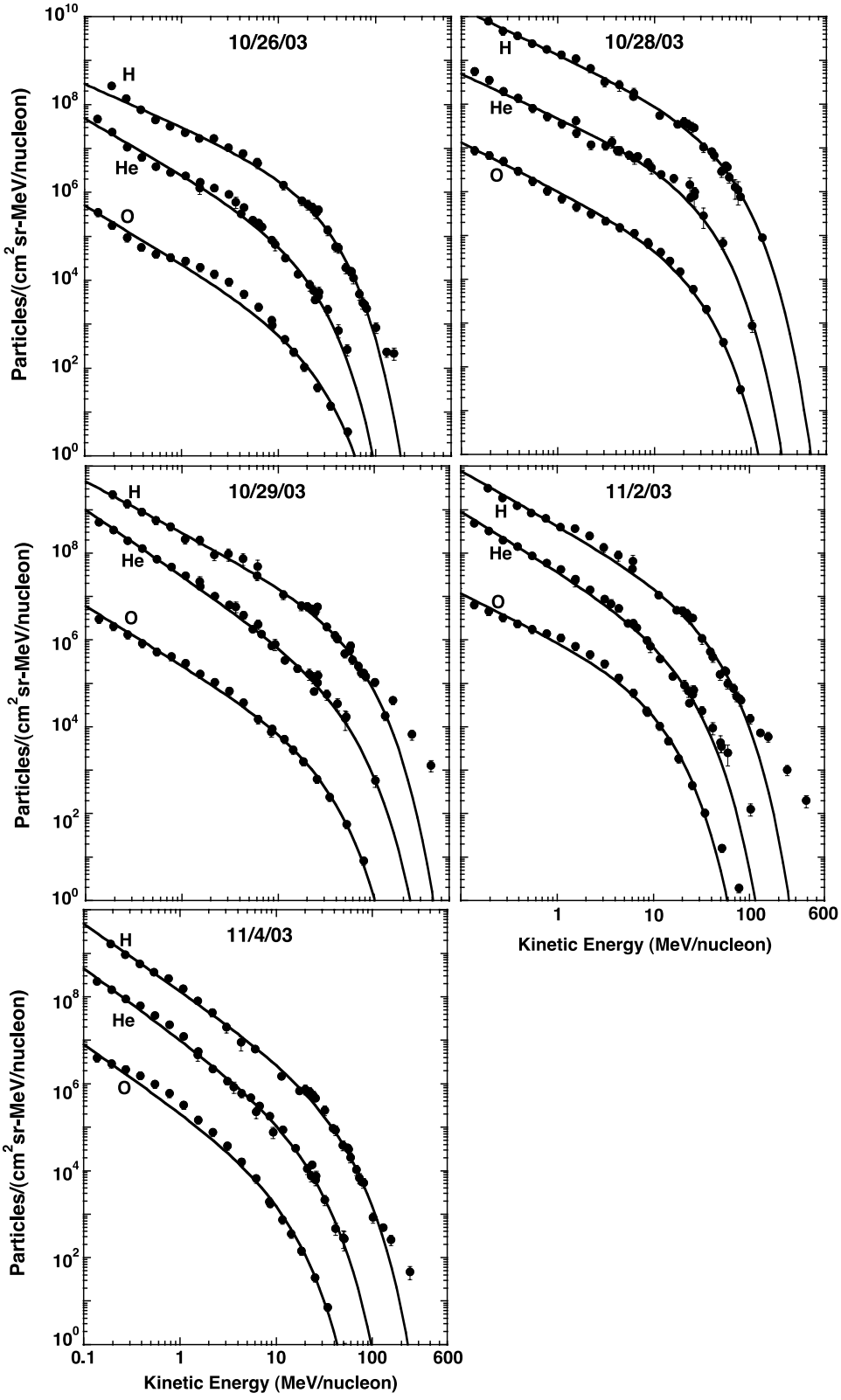

Figure 3. Fits to the fluence spectra of H, He, and O using the Ellison-Ramaty spectral shape (equation (1)) are shown for the five solar events. The data points are the same as in Figure 2.

spectra can also be represented as power laws. These spectra are similar in shape to many of the gradual SEP events that have been measured over a broad energy interval [*Mazur et al.*, 1992; *Mason et al.*, 1998; *Tylka et al.*, 2000, 2005], including, for example, the 14 July 2000 (Bastille Day) event [*Smith et al.*, 2001; *Tylka et al.*, 2001].

[16] In some of the events in this study there is a clear difference in fluence between protons measured in the

Table 4. Ellison-Ramaty Fitting Parameters

Event	Species	Normalization	Gamma	Eo
10/26/03	H	$3.20 \pm 0.19 \times 10^7$	-0.96 ± 0.04	15.0 ± 0.7
	He	$2.64 \pm 0.17 \times 10^6$	-1.26 ± 0.05	10.5 ± 1.0
	O	$2.43 \pm 0.15 \times 10^4$	-1.32 ± 0.04	13.2 ± 1.0
10/28/03	H	$1.35 \pm 0.09 \times 10^9$	-1.05 ± 0.04	28.2 ± 1.9
	He	$4.90 \pm 0.25 \times 10^7$	-1.00 ± 0.04	16.8 ± 0.9
	O	$1.06 \pm 0.05 \times 10^6$	-1.10 ± 0.04	13.9 ± 0.6
10/29/03	H	$2.98 \pm 0.18 \times 10^8$	-1.17 ± 0.04	33.1 ± 2.3
	He	$3.00 \pm 0.15 \times 10^7$	-1.52 ± 0.03	26.7 ± 2.5
	O	$2.67 \pm 0.14 \times 10^5$	-1.35 ± 0.03	16.3 ± 1.0
11/2/03	H	$4.34 \pm 0.27 \times 10^8$	-1.26 ± 0.04	20.2 ± 1.3
	He	$3.96 \pm 0.24 \times 10^7$	-1.36 ± 0.04	10.4 ± 0.9
	O	$9.88 \pm 0.63 \times 10^5$	-1.08 ± 0.04	6.25 ± 0.32
11/4/03	H	$1.39 \pm 0.08 \times 10^8$	-1.54 ± 0.04	22.9 ± 1.1
	He	$1.08 \pm 0.06 \times 10^7$	-1.62 ± 0.04	11.2 ± 0.8
	O	$2.34 \pm 0.16 \times 10^5$	-1.54 ± 0.03	6.66 ± 0.37

spacecraft frame by ULEIS and EPAM, with EPAM fluences systematically lower than those from ULEIS. For each of these events, as well as other events, we have examined the full three-dimensional proton angular distributions and determined that differences such as these are due to particle anisotropies. These differences are due mainly to the Compton-Getting effect [*Compton and Getting*, 1935], which will produce systematic streaming in the antisunward direction, especially at low energies and at high solar wind speeds. For example, in event 2 the solar wind speed exceeded 1850 km/s following the arrival of the shock on 29 October 2003 and it remained >1000 km/s for most of the following 2 days [*Skoug et al.*, 2004].

[17] In order to characterize these spectra further, we have fit them with several spectral shapes. *Ellison and Ramaty* [1985] proposed that solar particle spectra accelerated by shocks would have spectra of the form:

$$dJ/dE = KE^{-\gamma} \exp(-E/E_o), \quad (1)$$

where J is the intensity, E is kinetic energy/nucleon, and K, E_o, and γ are constants. This spectrum has a power law shape at low energies, as expected from shock acceleration, with an exponential rollover at high energies, presumably determined by the finite radius of the shock or the time available for accelerating particles to high energy. *Tylka et al.* [2000, 2001] have found this spectral form to be useful in characterizing the spectra of a number of SEP events.

[18] In Figure 3 we show the result of fitting the Ellison-Ramaty spectral form to these five events. In fitting these spectra over a broad energy interval, including data from several instruments, a 20% systematic uncertainty was added in quadrature with the statistical uncertainties (25% in the case of PET), which resulted in reduced chi-square values with a median value of 1.64. Table 4 includes the fitting parameters. The Ellison-Ramaty form can fit the low-energy portion of the spectra reasonably well, and it can also fit the breaks in the spectra. However, in a number of cases where the spectra extend to high energy, the fit rolls over too soon [see also *Mazur et al.*, 1992] and does not match the highest energy points (especially the proton spectra in events 3 and 4).

[19] *Tylka et al.* [2000, 2005; see also *Mazur et al.*, 1992] have shown that spectral breaks in SEP events such as these are ordered by the charge-to-mass ratio of the species, and they considered E_o functions of the form $E_o \sim (Q/M)^b$, with b typically ≈ 1 but occasionally as large as $b \approx 2$. In these five events, the $E_o(H)/E_o(He)$ ratios ranged from 1.2 to 2.0, with the last two events giving ratios very close to 2, as would be expected if b = 1. In all cases but one (oxygen in event 1), we find $E_o(H) > E_o(He) > E_o(O)$.

[20] The fact that the location of the spectral breaks is apparently ordered by Q/M suggests that the spectra might be better organized if plotted as a function of rigidity. In Figure 4, the data from the 2 November 2003 event have been plotted as differential rigidity spectra, assuming that Q(O) = 6.5. It is conceivable that in this representation the

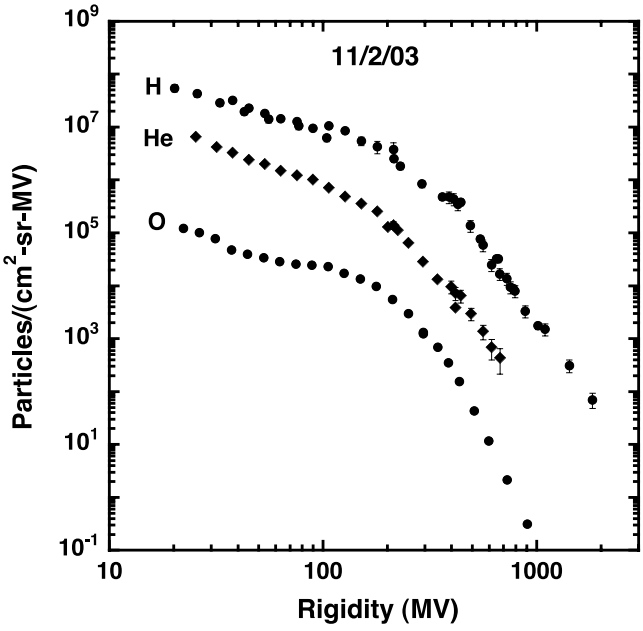

Figure 4. The fluence spectra from the 11/2/04 event are plotted as differential rigidity spectra. The data points are the same as in Figure 3, but they have been converted to differential rigidity measurements.

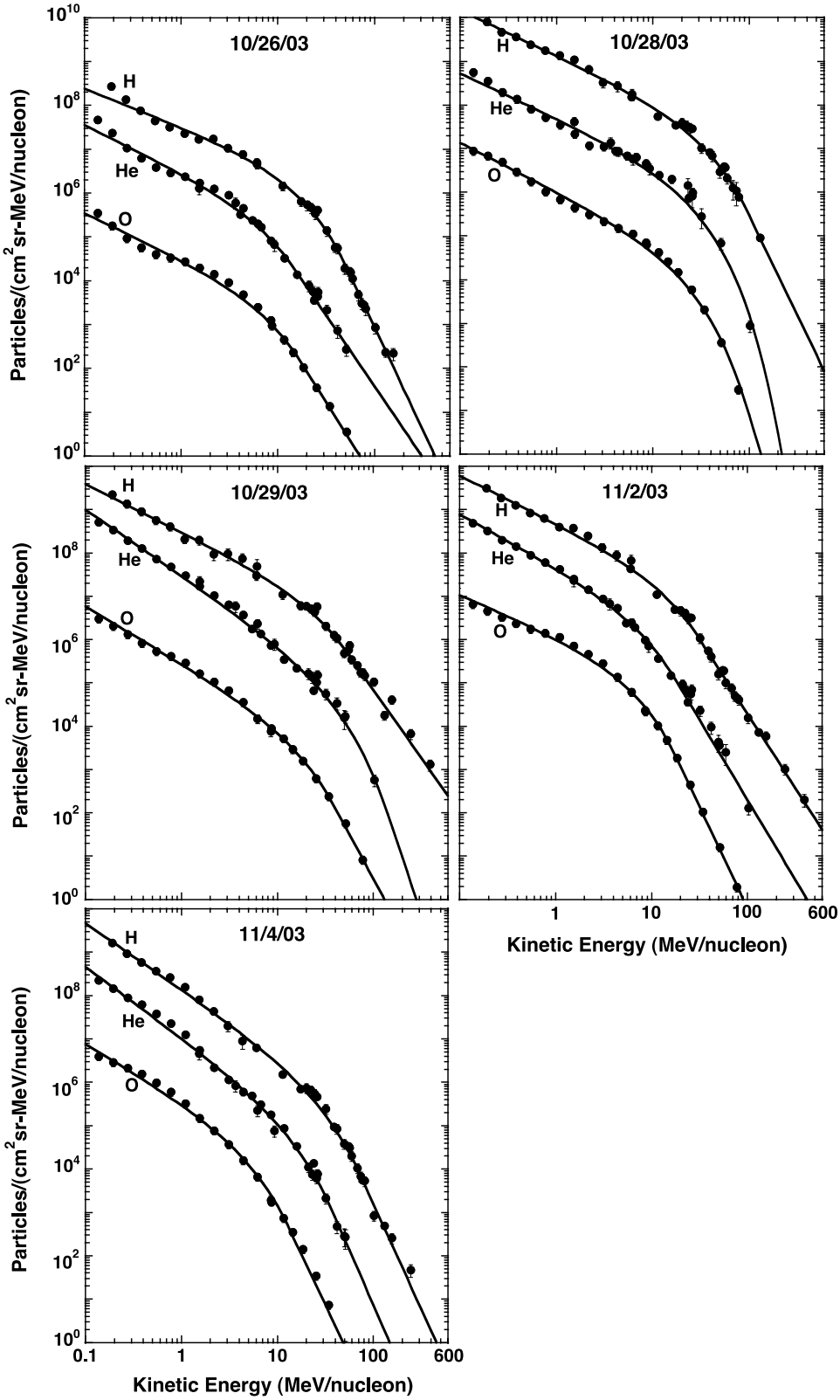

Figure 5. Fits to the fluence spectra of H, He, and O using the *Band et al.* [1993] spectral shape (equation (2)) are shown for the five solar events. The data points are the same as in Figures 2 and 3.

spectral breaks would occur at the same rigidity, but this was not the case in any of the five events.

[21] The Ellison-Ramaty form fails to fit the highest-energy proton points in several of the events, and it appears that a double power law representation might do a better job of fitting the spectra. In Figure 5 we show the results of fitting the H and He spectra with a spectral form developed by *Band et al.* [1993] to fit gamma-ray burst spectra, a form

Table 5. Fitting Functions for Double Power Law Spectra

Event	Species	Normalization	γ_a	γ_b	Eo
10/26/03	H	$3.26 \pm 0.20 \times 10^7$	-0.87 ± 0.06	-4.68 ± 0.20	12.8 ± 1.08
	He	$3.01 \pm 0.24 \times 10^6$	-1.08 ± 0.08	-3.24 ± 0.20	6.86 ± 0.9
	O	$3.20 \pm 0.25 \times 10^4$	-1.04 ± 0.07	-3.52 ± 0.15	6.99 ± 0.93
10/28/03	H	$1.35 \pm 0.09 \times 10^9$	-1.04 ± 0.04	-4.57 ± 0.93	27.4 ± 2.6
	He	$4.93 \pm 0.16 \times 10^7$	-1.03 ± 0.02	-11.0 ± 3.5	17.9 ± 0.5
	O	$1.04 \pm 0.04 \times 10^6$	-1.12 ± 0.02	-7.0 ± 4.0	15.0 ± 0.3
10/29/03	H	$3.05 \pm 0.20 \times 10^8$	-1.10 ± 0.05	-3.15 ± 0.14	26.1 ± 3.0
	He	$2.99 \pm 0.17 \times 10^7$	-1.52 ± 0.04	-6.6 ± 7.7	27.4 ± 4.9
	O	$2.82 \pm 0.17 \times 10^5$	-1.31 ± 0.03	-4.09 ± 0.38	14.0 ± 1.5
11/2/03	H	$4.89 \pm 0.33 \times 10^8$	-1.09 ± 0.06	-3.44 ± 0.10	13.2 ± 1.5
	He	$4.75 \pm 0.33 \times 10^7$	-1.22 ± 0.05	-3.70 ± 0.14	7.09 ± 0.76
	O	$1.21 \pm 0.09 \times 10^6$	-0.95 ± 0.05	-4.67 ± 0.15	4.87 ± 0.37
11/4/03	H	$1.40 \pm 0.09 \times 10^8$	-1.52 ± 0.04	-4.86 ± 0.33	21.7 ± 1.5
	He	$1.09 \pm 0.03 \times 10^7$	-1.62 ± 0.02	-5.06 ± 1.01	11.2 ± 0.3
	O	$3.77 \pm 0.34 \times 10^5$	-1.32 ± 0.05	-4.65 ± 0.12	3.90 ± 0.33

that has also been used by *Tylka et al.* [2005] to fit SEP spectra. The equation for this spectral shape is given by

$$dJ/dE = CE^{-\gamma_a} \exp(-E/E_o) \text{ for } E \le (\gamma_b - \gamma_a)E_o;$$
$$dJ/dE = CE^{-\gamma_b}\left\{[(\gamma_b - \gamma_a)E_o]^{(\gamma_b-\gamma_a)} \exp(\gamma_a - \gamma_b)\right\} \text{ for } E \ge (\gamma_b - \gamma_a)E_o, \quad (2)$$

where γ_a is the low-energy power law slope and γ_b is the high-energy power law slope and E and E_o are measured in energy/nucleon. The function is identical to the Ellison-Ramaty form below the transition energy, $(\gamma_b - \gamma_a)E_o$. At higher energies, the function makes a smooth transition to a second power law. It is clear that this spectral form gives an improved fit to the high-energy spectra, and the median reduced Chi-square for the fits to H, He, and O was 1.15, compared to 1.64 for the Ellison-Ramaty form. The parameters of the fits to these events are summarized in Table 5.

[22] Inspection of Table 5 shows that the E_o values are generally smaller for the heavier species, as is discussed further in section 4. On the other hand, it is less clear whether there is any systematic pattern to the values of γ_b. Although it is surprising that the He γ_b values are the most negative in three of the five events, notice that the uncertainties on the He γ_b values in these cases are relatively large because there are fewer high-energy measurements for He. It looks as if a quantitative study of the species dependence of γ_b for H, He, and O will await measurements with an improved determination of the spectra in the energy range from ~50 to 100 MeV/nucleon.

[23] The shapes of the fluence spectra are quite similar, as illustrated in Figure 6, which compares the fits to the five proton spectra. The 28 October 2003 event has the largest fluence below ~250 MeV, but at higher energies the spectral fits indicate that both events 3 and 4 have harder spectra. Events 2, 3, and 4 were all prominent ground-level events recorded in a number of neutron monitors (based on real-time data from the University of Delaware website http://neutronm.bartol.udel.edu//Welcome.html and John Bieber (personal communication, 2004).

3.3. H to He Ratios

[24] From inspection of Figure 2 it is clear that the relative abundance of H and He vary with energy and from event to event. This is further illustrated in Figure 7, which plots the H/He ratio as a function of time at ~10 MeV/nuc, and in Figure 8, where the H to He ratio is plotted as function of energy/nucleon for each event. In all these events the H/He ratio, in the energy range from 0.1 to 100 MeV/nucleon, varies by factors that range from ~3 to 50 [see also *Mazur et al.*, 1993]. Note that only in one case (event 2) is the trend of the data at ~2 MeV/nucleon consistent with the average SEP ratio of H/He = 27.5 derived by *Reames* [1995] by summing a large number of gradual SEP events in the energy interval from 1 to 4 MeV/nucleon. This is perhaps not surprising given that the H/He values are varying significantly with energy and from event to event. The sudden change in the H/He ratio near

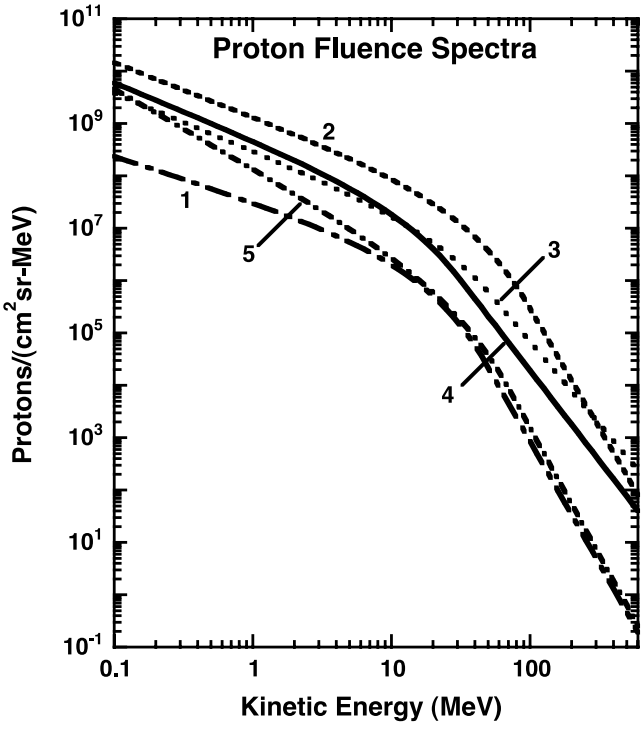

Figure 6. A comparison of the double-power law fits to the proton spectra for events 1 to 5. Note that the extrapolations of the fits extend somewhat higher in energy than the measurements (see Figure 5).

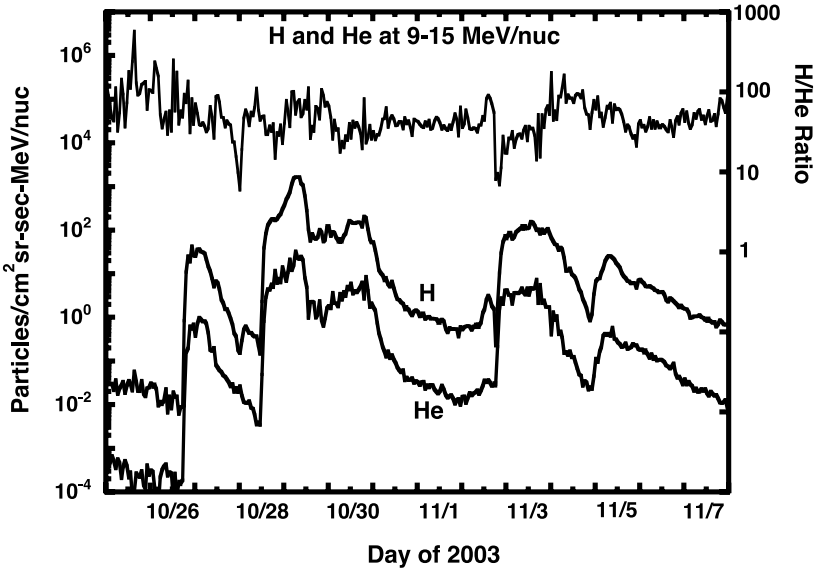

Figure 7. The intensities of 9 to 15 MeV/nucleon H and He are shown as a function of time, along with the resulting H/He ratio. The H data are from GOES-11 and the He data are from ACE/SIS.

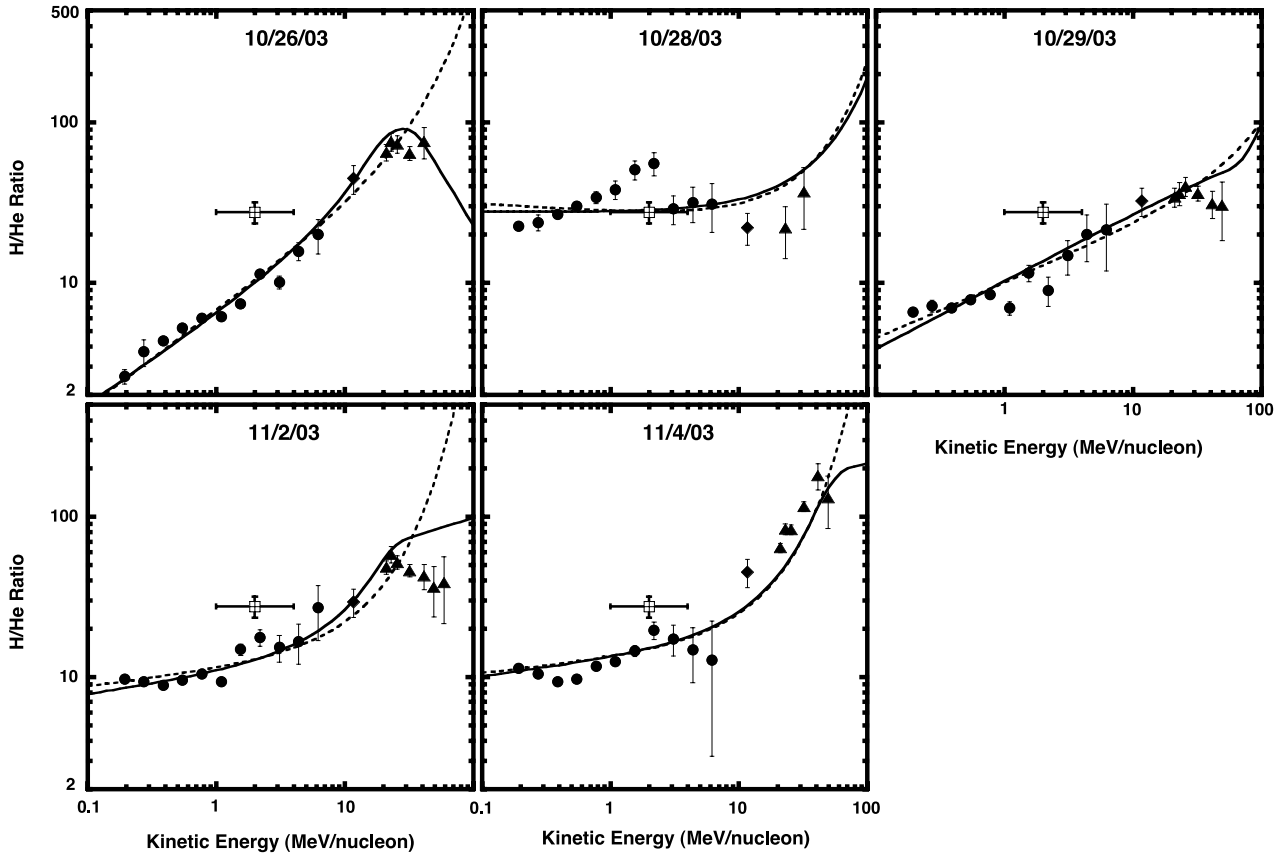

Figure 8. The H/He ratio measured in events 1 to 5 is shown as a function of energy based on data from ACE/ULEIS (filled circles), GOES-11 and ACE/SIS (filled diamonds), and SAMPEX/PET (filled upward triangles). The long-term average H/He ratio of SEPs at 1 to 4 MeV/nucleon derived by *Reames* [1995] is shown as an open square. Also shown are the H to He ratios that result from the fits to the spectra using the functions proposed by Ellison and Ramaty (dotted lines) and Band et al. (solid lines).

Table 6. Integrated Abundances From 0.1 to 100 MeV/Nucleon

Event	H/He	He/O
10/26/03	12.1	102
10/28/03	30.2	48
10/29/03	8.7	131
11/2/03	11.2	51
11/4/03	12.4	53

~20 MeV/nucleon in some of the events occurs because the break in the He spectra occurs at a lower energy/nucleon than the break in the H spectra (see Figures 3 and 5).

[25] Also shown in Figure 8 is the H/He ratio obtained from fits to the spectra using the Ellison-Ramaty and Band et al. spectral shapes. Although both spectra fits can represent the transition in the ratio from low to high energy, they sometimes differ greatly at higher energies, with the extrapolated Ellison-Ramaty fits suggesting that the He/H ratio continues to increase more than is indicated by the extrapolated Band et al. fits. This difference may have relevance to the extrapolation of SEP spectra of heavier species.

[26] The large variation of the He/H ratios with energy (Figure 8) raises the question of how one should characterize the relative abundance of H and He in these (or other) SEP events. The energy dependence observed in these five events argues against interpreting the observed ratio in any particular energy interval as a measure of the coronal composition, as was done by *Reames* [1995] for the average 1 to 4 MeV/nucleon abundances. Rather, it is likely that these very fast shocks accelerate a mixture of particles that includes coronal material, solar wind, and remnant suprathermal particles left over from earlier SEP events.

[27] Rather than select a particular energy or energy range for characterizing the relative abundances of individual SEP events, we have chosen to integrate the fluence spectra over energy to obtain the relative abundance of all accelerated particles that were observed. Table 6 includes the relative abundances of H, He, and O integrated from 0.1 to 100 MeV/nucleon. Note that except for the 28 October 2003 event, the H/He ratios are all ≈10. For comparison, the coronal H/He ratio is ~19 [*Laming and Feldman*, 2001] close to the average slow solar wind value of 23 and the fast solar wind value of ~19 [*von Steiger et al.*, 1998], while the photospheric H/He ratio is ~11.8 [*Grevesse and Sauval*, 1998; *Lodders*, 2003]. None of our events has an integrated H/He ratio that is close to the coronal value, and only the 28 October 2003 event has an integrated H/He ratio close to the average gradual SEP abundance ratio of 27.5 obtained by *Reames* [1995]. The integrated He/O ratios vary by a factor of ~2.5, with three events reasonably close to the gradual SEP value of He/O ≈ 57 from *Reames* [1995]. None of the measurements are particularly close to the average solar wind ratios of He/O ≈ 90 (slow wind) and He/O ≈ 73 (fast wind) obtained by *von Steiger et al.* [2000]. The reader is reminded that the coronal abundances of these three species (when compared with photospheric abundances normalized to Si) are depleted by a fractionation process that is generally thought to depend on either first ionization potential (FIP) or first ionization time (FIT) [see, e.g., *Geiss*, 1998]. Measurements of coronal and average solar wind abundances suggest that He is depleted somewhat more than H and O in the corona.

[28] The apparent overabundance of He in 4 of the 5 events, relative to coronal or solar wind values, suggests that either He is more easily accelerated than H, or that the source population is He-rich. This might be expected in event 1, which was preceded by a period enriched in ^{3}He (see section 3.6). *Mason et al.* [1999a] have suggested that small, impulsive, ^{3}He-rich events could provide a seed population of suprathermal ions that would be preferentially accelerated by CME-driven shocks. Such ^{3}He-rich events are also known to be enriched in ^{4}He relative to H [*Hurford et al.*, 1975; *Mason et al.*, 1999a].

3.4. Integrated Fluence Spectra of Electrons

[29] The electron intensities >2 MeV in Figure 1 indicate significant intensity increases in the first four of these events but a relatively smaller increase in the 11/4/03 event. The energy spectra derived at low energies from EPAM and at high energies from PET are shown in Figure 9. Both the low-energy and high-energy spectra are well represented by power laws. The low-energy power laws have $\gamma \approx -2$, while at >1.6 MeV the slope is more like −4. Because of the gap in the observations, we cannot determine where these spectra steepen. These low-energy spectra are similar in slope to those in the work of *Lin et al.* [1982] below ~200 keV, while the high-energy slopes are similar to those observed by *Lin et al.* [1982] above ~2 MeV and *Moses et al.* [1989] at even higher energies. In the study of *Lin et al.* [1982] and *Lin* [1985], the electron spectra were found to have a break around ~200 keV. Although the third and fourth spectral points in Figure 9 do indicate a steeper spectrum than the second and third points, the rather broad energy bins in Figure 9 make it difficult to compare these spectra in detail with those of *Lin* [1985] and *Lin et al.* [1982].

[30] The absolute magnitude of the high-energy spectra in events 2 and 3 is more uncertain because of the very significant dead time corrections that were needed at the times of maximum proton intensity. Indeed, during the early part of event 3 (see Figure 1) the PET live time decreased to a point where the electron intensity could not be reliably determined, and it was necessary to interpolate the intensity measurements to obtain the event-integrated fluence. Note in Figure 1 that the intensity of event 3 at MeV energies in PET appears to be significantly greater than that of event 2, while at EPAM energies these two events are of comparable intensity. We are confident that event 3 is the larger of the two at high energies, but it is possible that during this period some fraction (<50%) of the events are due to chance coincidences between two lower-energy electrons that independently trigger the first two detectors in PET, thereby mimicking the signature of higher-energy electrons. Although it appears that event 3 has a harder spectrum throughout the course of the event, we have not shown the PET spectrum for this event because of the possibility that chance-coincidence background contributes during the highest intensity portions of the event. The low-energy and high-energy electron spectra were fit separately with power laws of the form:

$$dJ/dE = kE^{-\gamma}, \quad (3)$$

where k is a normalization constant and g is the spectral index. The fitting parameters for these events are summar-

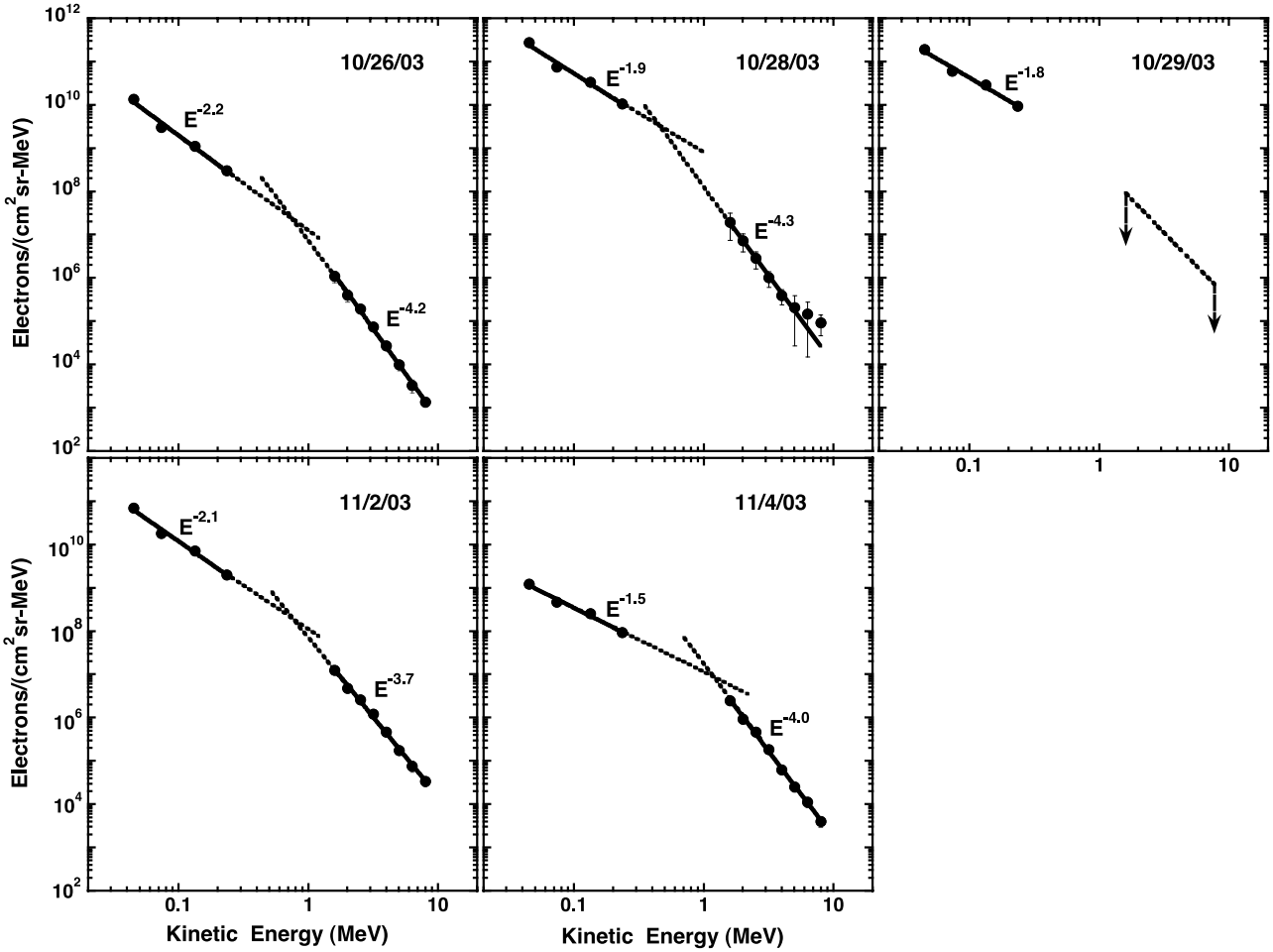

Figure 9. Energy spectra of energetic electrons in the five SEP events covered by this study, including 0.04 to 0.34 MeV data from EPAM/ACE and 1.8 to 8 MeV data from PET/SAMPEX. The slopes of power law fits to the low-energy and high-energy data are indicated. These fits have been extrapolated into the region of overlap (dotted lines). The high-energy data from the 29 October event are shown as upper limits because of possible background contributions (see text).

ized in Table 7, where the intensities are in units of electrons/cm^2 sr MeV.

[31] Although the electron and proton spectral shapes are similar, any possible relationship between the electron and proton spectral indices is difficult to determine from this limited sample of five events. *Lin et al.* [1982] report on nine large well-connected flare events and find an electron spectral range (0.01 MeV < E < 0.2 MeV) between −1 and −2, consistent with this study. When we compare the low-energy electron spectral index (Figure 9) to the proton spectral index >30 MeV, there is also a positive correlation, but the correlation is better between the spectral indices of the 1.8–8 MeV electrons and >30 MeV protons. *Lin et al.* [1982] selected only well-connected events, defined by flare locations between 30° and 90° solar longitude, while two of our events are near central meridian, which could introduce propagation effects. The five events in this study are an insufficient data base to study correlations of this kind, but we plan to extend these comparisons to additional events in the near future.

3.5. Total Particle Energy Content

[32] The fluence measurements presented here can be used to estimate the total energy content of energetic solar

Table 7. Fitting Parameters for Electron Spectra

	EPAM (0.04 to 0.32 MeV)		PET (1.6–8 MeV)	
Event	Normalization	Spectral Slope	Normalization	Spectral Slope
10/26/03	1.15×10^7	−2.23	8.40×10^6	−4.19
10/28/03	6.75×10^8	−1.90	1.46×10^8	−4.27
10/29/03	7.40×10^8	−1.76		
11/2/03	9.75×10^7	−2.08	7.24×10^7	−3.68
11/4/03	1.08×10^7	−1.50	1.67×10^7	−3.98

Table 8. Energy Content of Accelerated Interplanetary Particles

Event	Location[a]	CME Velocity,[b] km/s	CME Kinetic Energy, $\times 10^{31}$ ergs	Total Interplanetary Particle Energy, $\times 10^{31}$ ergs
10/26/03	N02W38	1537	35	0.14 + 0.21, −0.08
10/28/03	S16E08	2459	95	5.8 + 3.3, −2.1
10/29/03	S15W02	2029	7	1.6 + 2.5 − 1.0
11/2/03	S14W56	2598	120	3.8 + 8.4, −2.6
11/4/03	S19W83	2657	54	1.9 + 5.8, −1.4
4/21/02	S14W84	2397	18	2.8 + 8.4, −2.1

[a]Obtained from http://www.sec.noaa.gov/Data/index.html.
[b]*Gopalswamy et al.* [2005], *Emslie et al.* [2004], and A Vourlidas (personal communication, 2005).

particles in interplanetary space, as was recently done for the 21 April 2002 event by *Emslie et al.* [2004]. Following the approach in the work of Emslie et al., we have estimated the energy content of events 1–5, as tabulated in Table 8. The first step is to calculate the total particle energy per unit area escaping into the outer solar system at the location of Earth. To do this, we integrated the spectral fits in Figures 5 and 9 over the energy interval from 0.01 to 1000 MeV/nucleon. This integration included a correction for the average number of times that particles of a given energy crossed 1 AU as a result of scattering on the interplanetary magnetic field. This correction was based on simulations by J. Giacalone (personal communication, 2003) and by G. Li [see, e.g., *Li and Zank*, 2005]. Although these results involve extrapolation of the energy spectra down to ~0.01 MeV/nucleon, on average 98% of the energy content was between 0.1 and 100 MeV/nucleon where the fluences are measured. About 50% of the energy content was due to particles with >10 MeV/nucleon.

[33] It is also necessary to take into account the fact that the observed SEP intensity at Earth depends on the longitude and latitude where the event originated, and to integrate over the total area over which solar particles escape into the heliosphere beyond 1 AU. As explained by *Emslie et al.* [2004], this integration is based on a semiempirical model in which the maximum intensity is observed for events that originate at 0° longitude and 0° latitude. In this model, the intensities observed at Earth fall off exponentially with the latitude and longitude where the event originated, with e-folding angles in longitude of 25° for eastern events and 45° for western events (based on observations from GOES and ACE). By integrating over a 1-AU sphere centered on the Sun, it is possible to relate the observed fluence at Earth to the total energy content of accelerated particles in interplanetary space.

[34] The results in Table 8 show that four of the events during this time period involved total particle energies in excess of 10^{31} ergs, comparable to the 4/21/02 event studied by *Emslie et al.* [2004]. All of the events in Table 8 that total more than 10^{31} ergs involved CME velocities >2000 km/s. Although the observed fluences at Earth in the events 4 and 5 were significantly smaller than those for event 2, they were less favorably located (see Table 1) and the respective longitude corrections were factors of 2.4 and 4.9 times greater than for the centrally located 28 October 2003 event. There was a surprising amount of variation in these six events: the protons accounted for anywhere from 65% to 82% of the energy content, He varied from 10% to 19%, $Z > 2$ nuclei from 3% to 9%, and the electron contribution ranged from ~1% to ~18%.

[35] In the work of *Emslie et al.* [2004] it was estimated that the absolute uncertainty in these estimates could be as large as a factor of 4, mainly as a result of uncertainties in the SEP latitude and longitude distributions but also because of uncertainties in the correction for how many times particles cross 1 AU. The uncertainties in the five events in Table 8 were estimated by taking the square root of the multiplicative correction factor for multiple crossings of 1 AU and adding this in quadrature with the square root of the correction factor for latitude and longitude (thus a factor of 4 correction is assumed to have a factor of 2 uncertainty). The event-to-event uncertainty should be smaller than these estimates. Estimates of the total energy based on near-Earth measurements should be more accurate for events that originate near central meridian.

[36] Multispacecraft measurements using the two STEREO spacecraft along with ACE and SOHO could substantially reduce the uncertainties on both the SEP and CME kinetic energies in the future. For example, the approach of *Emslie et al.* [2004] uses an average longitudinal profile to represent all events, while in reality SEP events have a range of longitudinal widths. Data from STEREO will be very useful to determine how SEP longitude distributions might be estimated using observed CME widths.

3.6. Measurements of the ^{3}He/^{4}He Ratio

[37] Although ^{3}He is rare on the Sun, it has long been known that impulsive solar flares sometimes show enhancements of ^{3}He/^{4}He up to 10^4 times the solar value [e.g., *Reames*, 1999]. In large, CME-associated events such as the ones considered in this paper, significant enrichments of ^{3}He/^{4}He by factors of ~10 to ~100 are also often seen [e.g., *Cohen et al.*, 1999; *Mason et al.*, 1999b, 2002].

[38] Table 9 shows the ^{3}He/^{4}He ratios at ~1 MeV/nucleon measured by ULEIS for the five events in this study. Event 1 shows a factor of ~5 enrichment over the solar wind value, similar to several other particle events reported by *Mason et al.* [1999b], *Cohen et al.* [1999], and *Wiedenbeck et al.* [2000]. The upper limits for event 2 are rather high, due to the high background in this event, the

Table 9. ^{3}He/^{4}He Ratios

Event	^{3}He/^{4}He ($\times 10^4$) (0.5–2 MeV/nuc)
10/26/03	16 ± 8
10/28/03	<32
10/29/03	<9
11/2/03	<7
11/4/03	<6

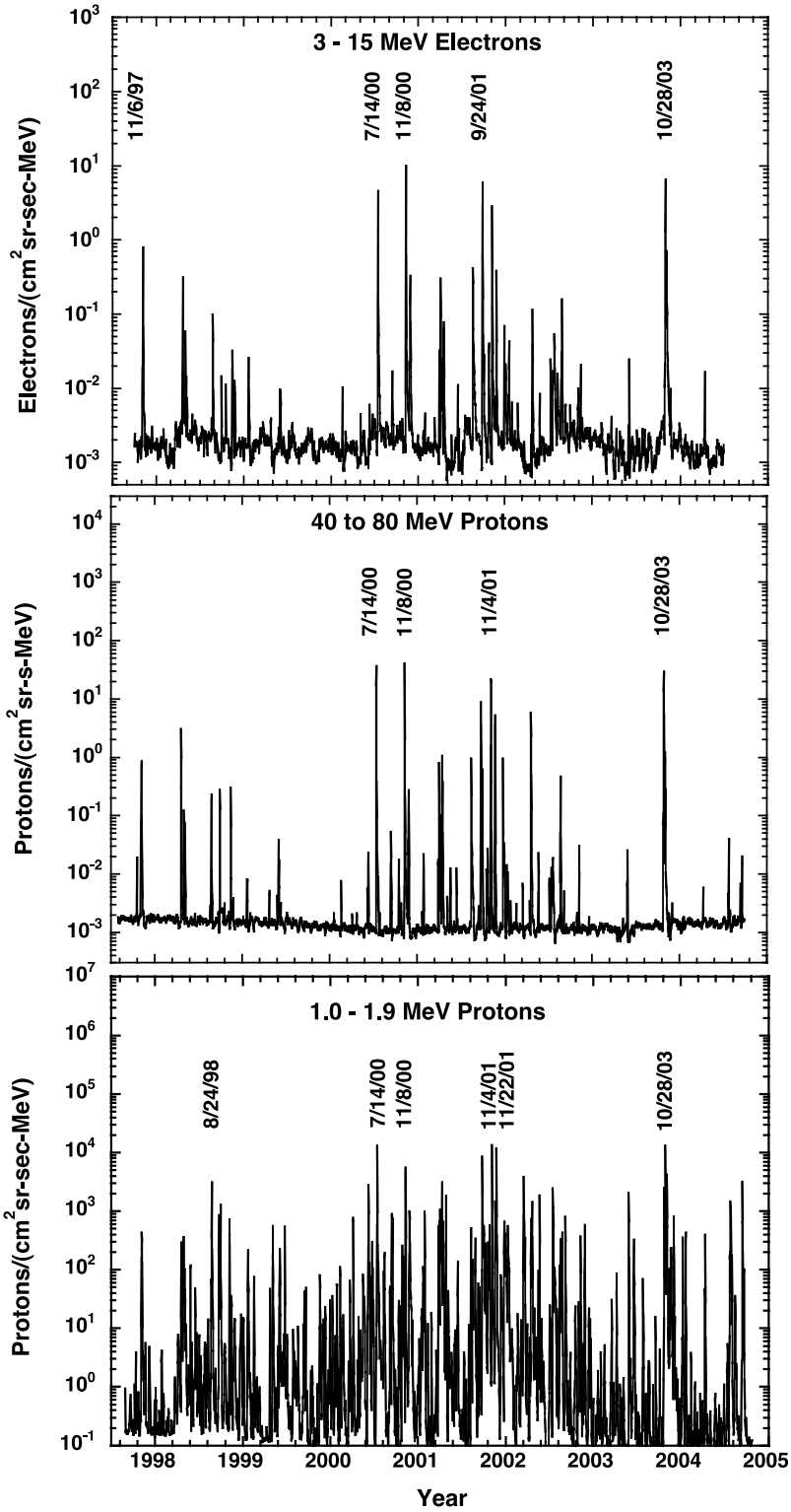

Figure 10. Daily averages intensities of: 3 to 15 MeV electrons measured by the PET/SAMPEX instrument (top panel); 40 to 80 MeV protons measured by GOES-11 (middle panel); and 1 to 1.9 MeV ions (mainly protons) measured by EPAM/ACE from late 1997 through late 2004 (bottom panel). The dates of some of the largest SEP events are indicated.

most intense of the group. Events 3–5 have upper limits of 1.5–2 times the solar wind value. The SIS instrument can measure ^{3}He in the 5 to 14 MeV/nucleon interval [*Cohen et al.*, 1999; *Wiedenbeck et al.*, 2000]. However, during these events only upper limits to the ^{3}He/^{4}He ratio were obtained.

[39] *Mason et al.* [1999b] argued that significant enrichments of ^{3}He in CME-related particle events were

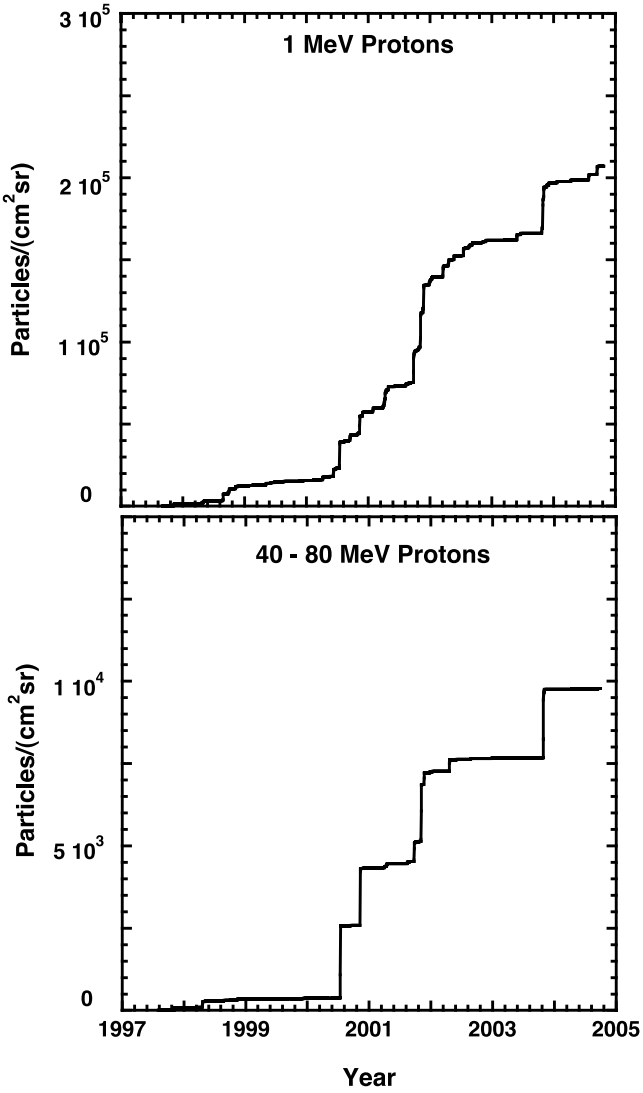

Figure 11. Fluences of 1 MeV protons (top panel, from EPAM/ACE) and 40 to 80 MeV protons (bottom panel, from GOES-11) integrated from October 1997 to late 2004.

due to reacceleration of ^{3}He from impulsive flares by the CME-driven shock. This association was made on a statistical basis. For the current set of events we note that there was significant ^{3}He from impulsive events present at 1 AU essentially continuously from 22 October through the onset of event 1 on 26 October. This may be the reason why the first event shows an overabundance of ^{3}He. The later events, for which the interplanetary medium was now filled with CME-accelerated material, would be expected to have little, if any, enhancement of ^{3}He, consistent with the observations.

3.7. October–November Events in the Context of Solar Cycle 23

[40] This past solar maximum has been one of the more active of the space age. Figure 10 illustrates that the 28 October 2003 event was among the three or four largest for both ~1 MeV and ~50 MeV protons and for 3 to 15 MeV electrons, comparable in intensity to the well-known 14 July 2000 (Bastille Day) event. Note that in the 40 to 80 MeV interval there are only seven events of this solar cycle with a proton intensity within a factor of 10 of the Bastille Day event, while at ~1 MeV there are many large events, including 15–20 with intensities within a factor of 10 of the Bastille Day event. There is clearly a different distribution of event fluences at 1 MeV/nucleon than at ~50 MeV/nucleon. This is further illustrated by the integral intensities shown in Figure 11. At ~1 MeV the proton intensity builds up rather slowly over the solar cycle in a series of many small steps [see also *Mewaldt et al.*, 2001]. The Bastille Day event accounts for ~10% of the solar cycle fluence at 1 MeV, while the series of October–November events accounts for ~15%. In the 40 to 80 MeV interval there is a series of larger steps, including three (the Bastille Day event, the 4 November 2001 event, and the 28 October 2003 period) that each account for ~20% of the solar cycle fluence.

[41] The 28 October 2003 event is one of the largest SEP events of the past 50 years (see, e.g., http://umbra.nascom.nasa.gov/SEP/seps.html). Figure 12 compares the spectra of the 28 October 2003 event with some of the largest of this solar cycle. The 28 October 2003 event is very similar in spectral shape and in intensity to the Bastille Day event that also originated near central meridian, where most of the largest SEP events in the past 30 years have originated. Indeed, four of the five events in Figure 12 have very similar spectral shapes; only the February 1956 event stands out because of its much harder spectrum (the spectrum for this event is based on balloon-borne and neutron monitor measurements).

4. Discussion

[42] It is interesting that all of the spectra in these five events can be represented by a common spectral shape, the

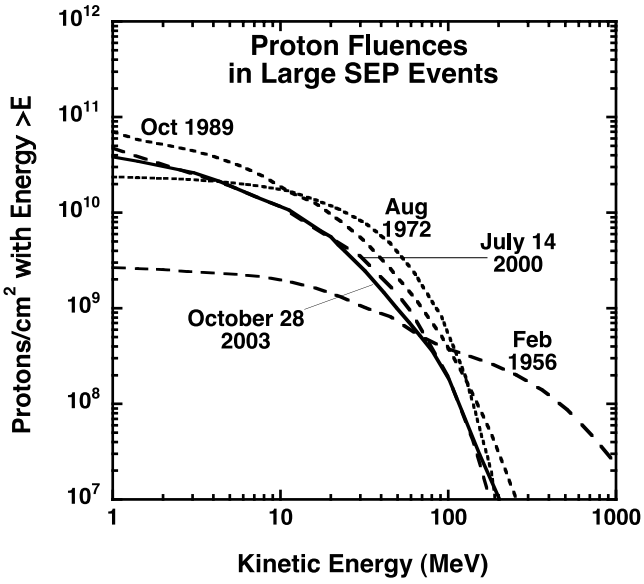

Figure 12. Proton fluence spectra are shown for some of the largest SEP events of the last 50 years. Spectra for the events prior to this solar cycle are adapted from *Turner* [1995]. The 14 July 2000 spectrum has been derived from data in the work of *Tylka et al.* [2001]. The 28 October 2003 spectrum is from this paper.

double power law with a break at energies that varies from a few MeV/nucleon to ~50 MeV/nucleon. The spectra of $Z \geq 6$ nuclei in these events can also be represented in this manner [*Cohen et al.*, 2005]. These spectral shapes are reminiscent of the spectra that result from the models of *Zank et al.* [2000, Figure 9] and *Li et al.* [2005], who have calculated numerically the acceleration of heavy ions at CME-driven shocks and their subsequent propagation in the interplanetary medium. These authors state that spectral breaks occur at the maximum energy to which the shock can accelerate particles, after which the acceleration efficiency drops significantly. In their model there is a spectrum of increased turbulence due to the waves generated by streaming protons escaping from the shock [*Lee*, 1983]. The maximum energy to which the shock can efficiently accelerate particles is set by the minimum wave number (k) at which there is enhanced turbulence; at lower k values the turbulence level drops and the resulting diffusion coefficient increases, allowing particles to escape from the shock much more easily. Because the shock weakens as it moves out from the Sun, the maximum energy decreases with time as the shock evolves [*Li et al.*, 2005].

[43] In those events where most of the fluence at 1 AU is associated with the passage of the CME-driven shock, the break in the fluence spectrum might be expected to correspond approximately to the maximum energy to which the shock can accelerate particles at 1 AU. *Li et al.* [2005] predict that the location of the breaks should scale as $(Q/M)^2$, with the breaks occurring at higher energy for species with greater Q/M values. We would expect similar behavior for particles responding to the turbulence spectra calculated by *Ng et al.* [2003], who calculated the spectrum of proton-amplified Alfven waves in large SEP events. In their calculations the proton-amplified Alfven waves produce a prominent bump in the wave spectrum that extends over 1 to 2 decades in wave number. In the inner heliosphere this bump results in a significant region of k-space with positive or near-zero slope [see *Ng et al.*, 2003, Figures 3, 4, and 5], analogous to that in the model by *Li et al.* [2005].

[44] *Mewaldt et al.* [2005] have examined the location of the break energies for nine species ranging from H to Fe and compared this energy with the charge-to-mass ratio of the ions as measured by SAMPEX. During the period just following shock passage in the 28 October event, the break energies for $2 \leq Z \leq 26$ nuclei could be fit by $(Q/M)^b$ with $b \approx 1.55$ to 1.75. The proton break energy was not consistent with the trend of the heavier nuclei, suggesting that protons may not be test particles in this event. In the 29 October 2003 event, the break energies showed much less dependence on Q/M, with a best-fit value of $b \approx 1$. It is possible that the spectra in the 29 October event were influenced by the fact that the CME was launched into a medium that was already highly turbulent as a result of the even larger event that occurred just 30 hours earlier.

[45] On the other hand, *Cohen et al.* [2005] suggest that the breaks in the spectra are most likely related to diffusion effects, and they suggest that relative positions of the breaks for different species should scale according to the diffusion coefficients, $\kappa = 1/3\ v\ \lambda$, where v is the particle velocity and λ is the mean free path. Assuming that λ is a power law in rigidity, or $(Mv/Q)^{\alpha}$, and that the breaks occur at the same values of the diffusion coefficient, they find the following scaling in energy between spectra for one element and another:

$$E_1/E_2 = \left[(Q/M)_1/(Q/M)_2\right]^{2\alpha/(\alpha+1)} \quad (4)$$

Using this relationship, Cohen et al. compared the spectra of seven species from O to Fe. Using average values of Q/M derived from <1 MeV/nucleon data, they found α values ranging from 0.8 to 2.7 for these five events, corresponding to Q/M scaling that ranged from $(Q/M)^{0.9}$ to $(Q/M)^{1.46}$.

[46] It is of interest to see if the breaks in the H and He spectra in these five events follow $(Q/M)^2$, as suggested by *Li et al.* [2005], or follow the scaling found by *Cohen et al.* [2005]. We have examined the relative location of the breaks for H and He in several ways. One measure of the break energy is the E_o value derived from fitting the Ellison-Ramaty spectral form (Table 4). If we compare the E_o values for H and He, we find that E_o for H ranges from 1.2 to 2 times that for He for these five events. On the basis of the suggestion of *Li et al.* [2005], we might have expected E_o for H to be 4 times that for He, since the ratio of their Q/M values is 2. It is possible that the expected behavior has been washed out to some degree because the fluence spectra include particles accelerated at different radii, with a range of maximum energies [*Li et al.*, 2005].

[47] We have also investigated the amount of energy shift in the He spectra that is required to minimize the variation in the He/H ratio. To determine this quantitatively, we used the results of the double-power law fits to the spectra (Figure 5 and Table 5), and restricted our attention to the energy range from 1 to 100 MeV/nucleon that is more or less centered on the breaks. Using this method and comparing energy shift factors of the form $10^{0.1n}$ with n an integer, we found that the optimum shifts ranged from factors of $\times 1.6$ to $\times 2.5$, corresponding to α values ranging from 0.5 to 2.

[48] In Figure 13 the proton spectra have been scaled down in energy by the amount indicated in the lower left-hand corner (and adjusted in intensity) so as to compare the proton shapes with both the measured and fit He spectra. Note that the agreement is essentially exact in events 2, 4, and 5, while there are some differences evident in events 1 and 3 (these differences would be anticipated just from inspection of Figure 5). For events 1 to 5, we find $\alpha = 0.5$, 0.5, 2, 2, and 1.4, respectively, while *Cohen et al.* [2005] find $\alpha = 1$, 2.4, 1.3, 0.8, and 2.7. Comparing these values and the resulting energy shifts, we find that there is a significant discrepancy only for event 2, where Cohen et al. found $\alpha = 2.4$ (corresponding to an energy shift of 2.7), and we find $\alpha \sim 0.5$ (corresponding to an energy shift of 1.6). In all but this case, the shifts derived from the α values of Cohen et al. would lead to a reasonable, if not optimum, correspondence between the H and He spectral shapes.

[49] As discussed by *Cohen et al.* [2005], the value of α can be related to the spectrum of interplanetary turbulence, assumed here to be a power law in wave number, or k^{-q}, with $\alpha = 2 - q$ [*Droege*, 1994]. The values of α derived here, ranging from 0.5 to 2, correspond to wave spectra varying from $k^{-1.5}$ to k^0, consistent with the range found by *Cohen et al.* [2005].

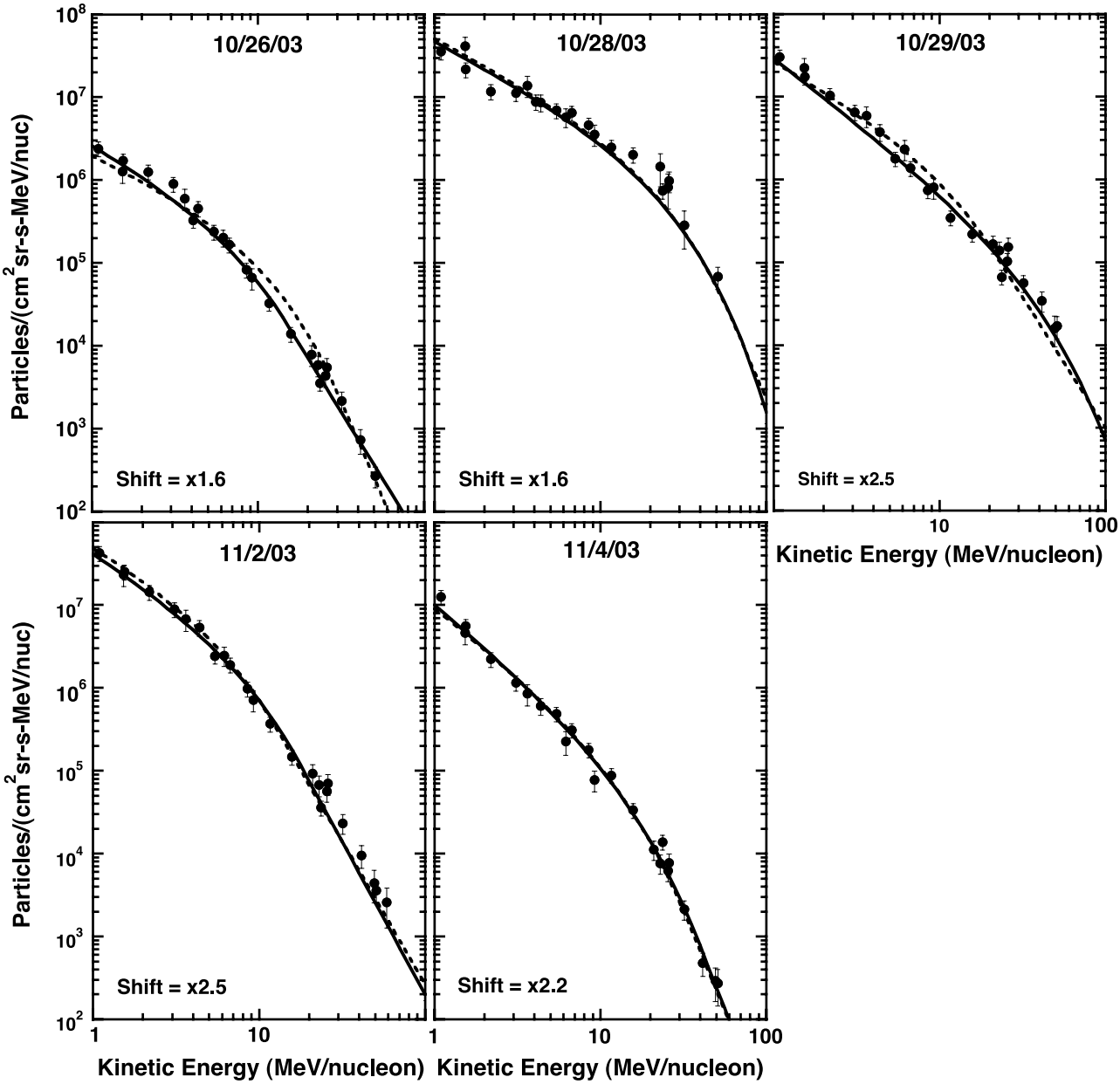

Figure 13. The double power law fits to the proton spectra are shifted in energy by the amounts indicated and adjusted in intensity to lie on the He data (dashed line). The fits to the He spectrum are shown as the solid line. In events 2, 4, and 5 the H and He fits are virtually indistinguishable.

[50] The above analysis and that by *Cohen et al.* [2005] suggest the presence of wave spectra with a slope significantly flatter than −5/3, with corresponding effects on the diffusion coefficient. Cohen et al. point out that wave spectra with just such characteristics have been presented by *Ng et al.* [2003], as discussed above. It is interesting that the region of positive slope in their wave spectra at 0.1–0.15 AU [*Ng et al.*, 2003, Figure 5] corresponds to proton rigidities from ∼100 to ∼300 MV (∼5 to 50 MeV), the same region where the breaks in the proton spectra are located (see Figure 5). This suggests that changes in the magnitude and slope of the interplanetary diffusion coefficient caused by proton-amplified Alfven waves may be responsible for the breaks in the spectra of the various ion species observed in these events.

[51] *Bamert et al.* [2004] have recently reported direct evidence for the presence of proton-amplified Alfven waves in large SEP events. Using data from ACE, they reported clear evidence for proton-amplified Alfven waves in wave spectra measured upstream of the shock in the 14 July 2000 (Bastille Day) event and also observed the effects of these waves on proton spectra measured by SOHO. They report that "The power spectral density is almost flat in the range from k = 0.25 k(1 MeV) to k = 2.5 k(1 MeV)…." (This range corresponds to proton energies from ∼0.16 MeV to ∼16 MeV). Subsequently, *Kallenbach et al.* [2005] have reported the presence of similar proton-enhanced wave spectra in measurements by ACE during the 11/2/03 event (our event 4). In the range from $\sim 10^{-8}$ to 10^{-7} m^{-1} we estimate their spectrum to be $\sim k^{-1}$. In this event we derive

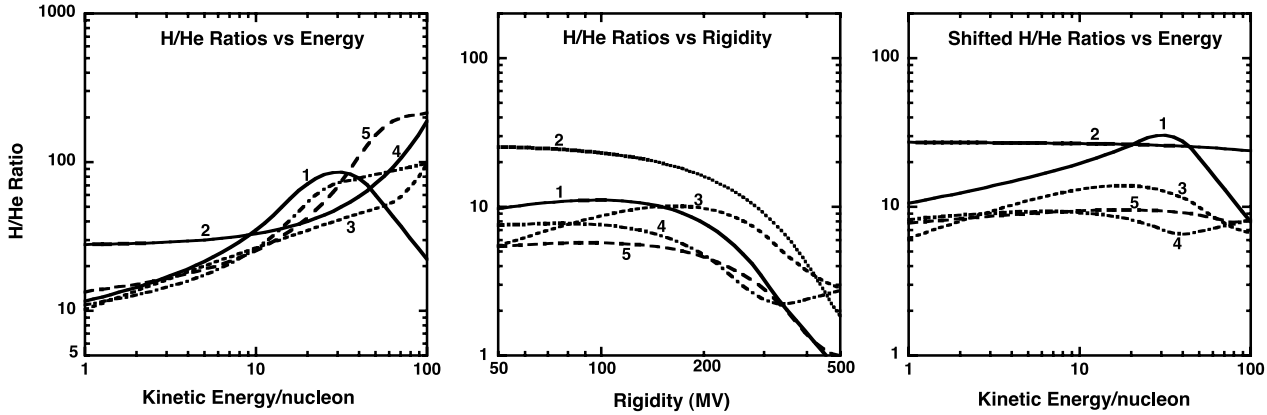

Figure 14. The ratio of the double power law fits to H and He (Figure 5) is shown for three different approaches to computing the H/He ratio. The left panel shows the ratio of the fits in Figure 5 as a function of kinetic energy per nucleon for events 1 to 5. In the middle panel the fits were converted to differential rigidity spectra before computing H/He as a function of rigidity. In the right panel the He spectra were shifted in energy by factors chosen to minimize the variation in the H/He ratio over the energy interval from 1 to 100 MeV/nucleon. The H/He ratios were then recalculated and multiplied by the shift factors indicated in Figure 13. The vertical scale is a factor of 200 in each case; note that the variation in H/He in the individual events is minimized in the right panel.

$\alpha = 2$ which corresponds to a wave spectral index of q = 0, while *Cohen et al.* [2005] derive a wave index of −1.2. We would expect that the wave spectra would be somewhat flatter nearer the Sun (where most protons >10 MeV originate) than at 1 AU. We conclude that wave spectra similar to those inferred by our analysis and that of Cohen et al. do exist in large SEP events. The reader is reminded that proton-generated wave spectra are dynamic features, resulting from particle transport, which evolve with time and with radius [see *Ng et al.*, 2003, Figures 2–5]. As pointed out by these authors, wave growth is very strong in the inner heliosphere but diminishes quickly with radius. As a result, these wave spectra can play an important role while the shock is close to the Sun, but they are usually not observable at 1 AU.

[52] This comparison of the H and He spectral shapes in these five events does not seem to fit a consistent pattern in which the ratio of the H and He break energies is a constant. In particular, the H and He fluence spectra do not fit the $(Q/M)^2$ scaling predicted by *Li et al.* [2005]. Rather, these results appear to be similar to those of *Cohen et al.* [2005], where the ratio of the break energies varies somewhat from event to event. Perhaps the fact that these fluence spectra include particles accelerated over a range of distances from the Sun has washed out the expected behavior to some extent. However, it may be that the proton spectra in these large events do not follow the same scaling as heavier ions because they are not test particles [*Ng et al.*, 2003; *Bamert et al.*, 2004; *Li et al.*, 2005]. It is also possible that processes other than those discussed here influence the shapes of these spectra and their scaling properties.

[53] A comparison of the H/He ratios for the five events is shown in Figure 14, plotted versus energy, rigidity, and energy after scaling the He spectrum up by the shift factors chosen to minimize the percentage variation in the H/He ratio as a function of energy/nucleon (see Figure 13). Plotting the spectra as rigidity spectra does not reduce the overall variation in the H/He ratio, but it does reduce the variation for rigidities less than ∼250 MV (∼30 MeV for protons), which generally corresponds to the region below the spectral breaks. Shifting the He spectra by the amounts indicated in Figure 13 reduces the amount of variation in the H/He ratio substantially.

[54] It is of interest to compare the total energy content of the SEPs observed in these events with the total kinetic energy of the individual CMEs, which have been reported by *Gopalswamy et al.* [2005]. This comparison is shown in Figure 15. Note that the SEP kinetic energies range from ∼0.4% to 24% of the CME kinetic energies, similar to the 21 April 2002 event analyzed by *Emslie et al.* [2004]. If we assume that the energy content of the particles comes mainly from particle acceleration at the CME-driven shock, we can conclude that the shock acceleration process has a variable efficiency, which at times must be very efficient, such that the production of energetic particles sometimes extracts a reasonably large percentage (∼10% or more) of the CME kinetic energy. It is interesting that galactic cosmic rays apparently extract a similar fraction of the kinetic energy from supernova shocks in order to sustain the energy density of cosmic rays in the galaxy (∼1 eV/cm^3) over the average cosmic ray lifetime of ∼15 million years [*Yanasak et al.*, 2001].

[55] Of course, it is also possible that some of the observed particles were accelerated at the flare site by other energy sources [see, e.g., *Cane et al.*, 2003] or that some flare-accelerated particles were further accelerated by the shock [*Mewaldt et al.*, 2003; *Li and Zank*, 2005]. In these cases, the efficiency estimates could be reduced to some extent. Of course, the uncertainties in the comparison in Figure 15 are still rather large. However, these five events all involved very fast CMEs, and they originated over a range of longitudes. The uncertainties in the SEP estimates are minimized for events that originated near the central meridian, while the uncertainties in the CME kinetic energy estimates are minimized for those events that originated near the limb (N. Gopalswamy and A. Vourlidas, personal

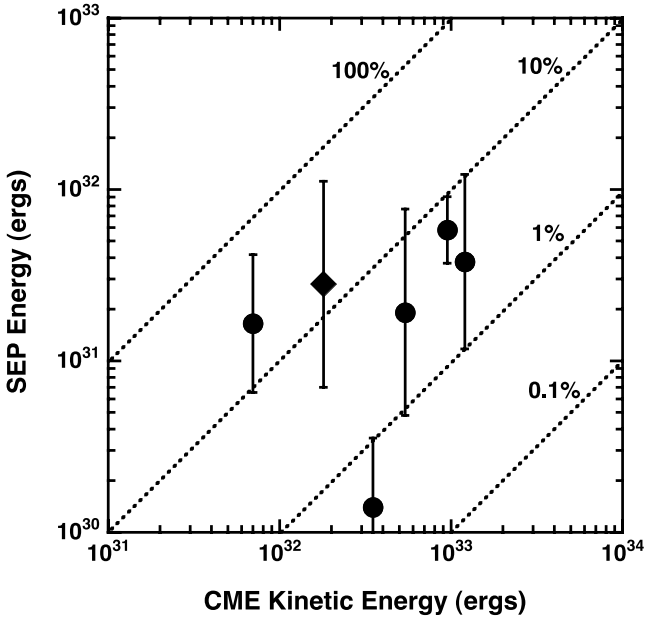

Figure 15. The total SEP kinetic energy of the five events from late 2003 (see Table 9) is plotted versus the CME kinetic energy [*Gopalswamy et al.*, 2005; A. Vourlidas, personal communication, 2005]. Also shown is the 21 April 2002 event (diamond) from *Emslie et al.* [2004]. Although *Gopalswamy et al.* [2005] did not provide uncertainties for their CME kinetic energies, *Emslie et al.* [2004] estimate a factor of ~2 uncertainty for the 21 April 2002 event.

communication, 2005). We hope to extend this study to a number of additional events in the near future.

5. Summary

[56] By combining data from five instruments on three different spacecraft, this study has produced measurements of H, He, and O spectra extending from ~0.1 to 100 MeV/nucleon and electron spectra from 0.04 to 8 MeV during five large SEP events within a 9-day span. The energetic particle fluences in this period constituted a significant fraction of solar particle production during solar cycle 23, anywhere from ~10% to ~25%, depending on energy. The 28 October 2003 event, in particular, was comparable in fluence to some of the largest events observed during the space age.

[57] The spectral shapes in all five events can be represented as double power laws, with low-energy slopes ranging from −1 to −1.5 and high-energy slopes that typically ranged from −3 to −5. The transition between these power laws occurs between ~5 and ~50 MeV/nucleon. The double-power law representation of *Band et al.* [1993] was found to provide a better fit to these spectra than the more conventional spectral form due to *Ellison and Ramaty* [1985]. This shape is also characteristic of many of the other large events of the last 50 years.

[58] In all cases the breaks in the H spectra occurred at higher energies than the breaks in the He and oxygen spectra. In the CME-driven shock-acceleration model of *Li et al.* [2005], the location of such breaks is expected to scale as $(Q/M)^2$, implying a factor of four difference in energy for H and He. The observed difference in the break energies, determined by shifting the individual H and He spectra in energy until they matched, amounted to more like a factor of 2 ± 0.5. However, it is also possible that the model of Li et al. does not apply in these large events because protons may not act as test particles, as it is the protons that are responsible for producing most of the turbulence essential to the shock acceleration process.

[59] The difference in the H and He break energies can also be interpreted as a result of diffusive processes, as proposed by *Cohen et al.* [2005]. In this case the typical factor of two difference in break energies can be interpreted as arising from a diffusion coefficient that scales as $(Q/M)^{\alpha}$, with $\alpha \approx 1$, suggesting wave spectra with a relatively flat slope in the range corresponding to rigidities near ~100 to ~300 MV, where the spectral breaks are located. It is possible that proton-generated Alfven waves, such as those predicted by *Lee* [1983] and *Ng et al.* [2003] and observed by *Bamert et al.* [2004] and *Kallenbach et al.* [2005], are responsible for the changes in wave spectra that we infer. If such features in the wave spectra are indeed present in these events, the resulting features in the interplanetary diffusion coefficient may be responsible for the spectral breaks and the Q/M scaling that we observe. Of course, it is also possible that other processes are responsible for the spectral scaling reported here for H and He and for heavier nuclei by *Cohen et al.* [2005].

[60] The electron spectra in these events can also be represented as double power laws, with typical low-energy spectral indices of −2 and typical high-energy indices of −4, consistent with earlier studies. Electrons accounted for anywhere from ~1% to 18% of the accelerated particle energy in these events. It will require a larger sample of events to explore how the electron and ion spectral shapes may be related.

[61] The He/H ratio in these events varied by a factor of ~5 to ~20 with energy. The total abundance of H and He integrated from ~0.1 to 100 MeV/nucleon varied from ~9 to 30, with four events having H/He ratios of ~10, none very close to the coronal abundance ratio of ~19, and only one close to the average gradual SEP event value of 27.5. It may be that He is more efficiently injected into the acceleration process than H because of its greater rigidity or that the source material was He-rich.

[62] Four of the five CMEs responsible for these events had velocities greater than 2000 km/s and all five of the associated shocks were still accelerating particles by the time they reached 1 AU. In these five events the estimated energy content of accelerated interplanetary particles amounted to $\sim 10^{31}$ ergs, accounting for a significant fraction (~0.4% to 24%) of the kinetic energy of the associated CMEs. Although there are uncertainties in these estimates, it appears that shock acceleration by CME-driven shocks can be a surprisingly efficient process. In the near future we plan to extend the studies in this paper to a number of other large events from solar cycle 23.

Appendix A: Instrument Descriptions and Data Analysis Issues

[63] In this appendix we provide a more complete description of the five instruments used in this study. We

also discuss some of the intercalibration issues that arose in trying to combine data from these instruments during some of the largest SEP events of this solar maximum.

[64] Ion measurements in the range ~0.1 to 8 MeV/nucleon were made using the Ultra-Low Energy Isotope Spectrometer (ULEIS) on ACE [*Mason et al.*, 1998]. ULEIS is a time-of-flight mass spectrometer that identifies ion mass and energy by measuring the time of flight of ions over a 0.5 m flight path along with the kinetic energy deposited by the ion in an array of solid state detectors. The instrument design emphasizes a combination of high resolution and large geometrical factor (~1 cm^2 sr). Although the triggering efficiency of ULEIS is ~100% for C and heavier ions, H and He have low efficiencies. These efficiencies were determined prelaunch at accelerator runs but require recalibration in flight due to losses in microchannel plate gain that are compensated from time to time by increasing the high voltage bias on the plates. During the events discussed here, the peak efficiency at 200 keV/nucleon was ~2% for H and ~15% for He, decreasing at higher energies. The ULEIS H efficiency used here was obtained from an intercalibration of ULEIS and EPAM H intensities during the SEP event of 24 August 2002, when anisotropies were low. The ULEIS He efficiency for the events in this paper was based on direct comparisons with SIS high-energy He and at lower energies by assuming similar ULEIS He and O spectra during portions of the decay phase of seven gradual SEP events observed between 22 April 2002 and 2 December 2003 (the assumption of spectral similarity during such periods is based on invariance of spectra late in gradual SEP events [*Reames et al.*, 1997]).

[65] During periods of very high intensity, such as those considered in this paper, instrument saturation and dead time issues are a potential problem. These were largely avoided during this period by the instrument's automated door, which closes off portions of the aperture depending on particle count rates in the telescope. For event 1, the door was 100% open; for events 2, 3, and 4, it was at its 1% open setting; for event 5 it was at its 6% open setting. The 26 October 2003 event was of moderate intensity and so presented no problems, and the subsequent door closures prevented saturation or dead time problems in events 3, 4, and 5. However, high-energy particles penetrating the telescope walls during much of event 2 led to very high count rates even though the door was at its 1% open setting. Between approximately 1020 UT on 28 October and 1300 UT on 29 October, ULEIS had significant dead time, which peaked at just over 80% between 2230 on 28 October and 0330 on 29 October. The dead time correction for ULEIS was obtained by comparing oxygen intensities with SIS oxygen intensities in overlapping energy intervals.

[66] The Solar Isotope Spectrometer (SIS) on board ACE consists of two identical silicon solid-state detector telescopes with a combined geometry factor of 38 cm^2 sr [*Stone et al.*, 1998a]. SIS measures the elemental and isotopic composition of particles with atomic number, Z, between 2 and 30 with energies of ~10 to ~100 MeV/nucleon using the dE/dx versus residual energy technique.

[67] The SIS instrument is mounted on the top (sunward facing) deck of ACE with its boresight tilted 25 degrees from the normal to the deck. The spacecraft rotates with a ~12 s period about this normal, and SIS has a 95° full-angle field of view, so during each rotation SIS views particles within a 145°-wide cone centered on the spin axis. During ACE's orbit about the L1 Lagrange point, the spin axis is pointed to within 5° to 15° of the Sun. Thus for example, when the interplanetary magnetic field direction is at its nominal 45° angle from the spacecraft-Sun line, the field direction is anywhere from 12.5° to 52.5° inside the edge of the spin-averaged field of view of SIS.

[68] SIS uses a priority system to select events to be preferentially telemetered during large SEP events, when the analyzed event rate often exceeds the telemetry capacity of ~10 events per second, with heavy ($Z > 3$) nuclei given higher priority than He. Furthermore, to minimize the instrument dead time that the large flux of H and He would cause during large SEP events if all these particles were analyzed, a timer is started after the analysis of a He ion to prevent the analysis of another such particle for an adjustable period of time (typically ~10 s). This design deliberately throttles the throughput of He particles to a few percent of the analyzed events under high-rate conditions. As a result, the live time correction factors to obtain the He intensity can become quite large. The SIS and GOES-11 energy ranges for He overlap. During four of the events under study there was excellent agreement between SIS and GOES-11 He intensities, but during event 2 (by far the largest during this period; see Figure 1) the He intensities measured by SIS were lower than those from GOES-11 by a factor of ~2.4. We have assumed that this discrepancy is due to an uncertainty in the He live time in SIS and corrected the SIS He fluences in Figure 4 to agree with those reported by GOES-11.

[69] The Electron, Proton, and Alpha Monitor (EPAM) on ACE [*Gold et al.*, 1998] is designed to measure ions ($E >$ 40 keV) and electrons ($E > 30$ keV) from five separate solid-state detector (SSD) telescopes oriented to give nearly 4π angular coverage. Ion elemental abundances are determined by a ΔE versus E telescope using a thin (4.8 μm) front detector in a three-component telescope. Two Low Energy Foil Spectrometers, LEFS60 pointing at 60° to the ACE spin axis and LEFS150 pointing at 150° to the spin axis, utilize a thin foil to prevent incident ions ($E < 350$ keV) from reaching the SSD while electrons can penetrate the foil with little energy loss. In the two Low Energy Magnetic Spectrometers, LEMS30 and LEMS120 pointing at 30° and 120°, respectively, electrons below ~315 keV are swept away from the solid-state detectors by a rare Earth magnet. In the LEMS30 telescope these magnetically deflected electrons are counted by an additional SSD. Owing to elevated backgrounds in the LEMS30 ion observations [*Haggerty et al.*, 2005], this study uses ion measurements from the LEMS120 telescope and electron measurements from the LEMS30 telescope.

[70] For large SEP events such as those in this study some electrons can scatter past the magnetic deflection system (at the ~5% level) and be falsely identified as low-energy ions. This is readily identified during the onsets of SEP events when the intensity in some low-energy ion channels rises prior to what ion propagation from the Sun would allow. For the fluence measurements in this study, the low-energy ion fluence is dominated by the intensity around the time of the

shock and electron contributions to the ion fluences are well below 1%.

[71] The Proton/Electron Telescope (PET) was launched into a 600 km near-polar Earth orbit aboard SAMPEX in July 1992 [*Cook et al.*, 1993]. PET consists of twelve 2- to 3-mm thick silicon solid-state detectors grouped into eight functional units to form a multielement telescope. Through a combination of range information in the stack and pulse-height information from the first three detectors, PET distinguishes protons, alphas, and electrons cleanly from one another, and provides energy spectra above 19 MeV/nucleon for protons and alphas and electron spectra from ~1.6 to 8 MeV. Pulse-height information is telemetered for only a sample of particles entering the telescope. A multiple dE/dx technique can be used to obtain energy spectra for ions that penetrate the entire detector stack; however, the need to use the pulse-height-analyzed sample to obtain spectra limits the statistical accuracy. Since H and He events are assigned the same priority, most of the ion events in the telemetry are protons, and it is not possible to obtain adequate statistics for the He spectrum beyond ~100 MeV/nucleon.

[72] Included in the PET telemetry is a "live time" counter, used extensively to obtain corrections for instrument dead time in the inner radiation belt [*Looper et al.*, 1996], mostly due to the high count rate in the front detector. However, count rates over the poles during the largest SEP events are much greater than in the inner radiation zone, and PET intensities for the October–November events are found to be systematically lower than GOES and SIS measurements after correcting for PET dead time using our standard algorithms. Since dead time affects measurements of all species and energies equally (as a common multiplicative factor), this problem does not impair measurements of spectral shape or of relative particle abundances, and therefore PET observations have simply been scaled upward by a factor that varies from event to event, in order to normalize PET observations with those from other instruments. These factors, independent of energy and species, varied from $\times 2$ in event 4 to $\times 7$ in event 2, the most intense of this series. It is possible that other factors contributed to these discrepancies. For example, it is possible that PET measures lower SEP intensities due to geomagnetic effects (PET is at a much lower altitude (~600 km) than GOES-11 (~40,000 km)). Perhaps SEPs do not always have access over the full view cone of PET (~50° full angle) for all portions of each polar pass.

[73] The electron response of the PET instrument was calibrated prior to launch using accelerator and beta-spectrometer facilities covering electron energies from ~0.5 to 30 MeV. This study includes events that trigger the first two or three PET detectors in coincidence. Calibration data in 16 energy intervals ranging from ~1.6 to 8 MeV were integrated over angles to provide omnidirectional response functions. Flight data from invariant latitudes >75° were collected in the same energy intervals and averaged over each polar pass, thereby providing ~48 min time resolution. With interpolation between the polar passes, the data were integrated over the duration of each SEP event to obtain a fluence for each energy channel.

[74] During times of intense solar protons a few of the electron channels are contaminated by a background of degraded proton signals (e.g., protons passing through the edge regions of the two front detectors, P1 and P2). An estimate of this background is obtained from energy channels without a normal electron response and subtracted from the data. A model electron fluence spectrum is constructed with eight points logarithmically spaced in energy from 1.6 to 8 MeV and connected by power law segments. This spectrum is combined with the calibrated response functions and integrated over energy to obtain simulated counts in each channel. The spectral points are then adjusted to obtain a least squares fit between the simulated and observed counts, while simultaneously satisfying a smoothness constraint on the spectrum. The data points are weighted according to the sum of the statistical uncertainties and an additional 20% relative uncertainty on each point. The smoothness criterion and the additional relative uncertainty are required to overcome influences of systematic uncertainties in the instrumental response and in the background corrections. Uncertainties in the final spectral points are estimated by error propagation of the assumed weighting factors divided by the mean square mismatch between the simulated and observed data points in order to approximately account for systematic discrepancies.

[75] At any given time there are usually SEP data available from two or more GOES satellites. In comparing the solar proton intensities reported by GOES-10 and GOES-11 in a number of large SEP events between 2000 and 2003, we found that GOES-10 measurements were systematically lower than those from GOES-11 by an energy-dependent factor that was sometimes as large as ~2 at ~10–20 MeV and less at higher energies. This study has been restricted to GOES data from GOES-11. The GOES-10 vehicle was inverted relative to the other GOES spacecraft because of a problem with its solar array (T. Onsager, personal communication, 2001). The inversion forced the Energetic Particle Sensors on GOES-10 to look toward the east rather than the west. Thus particles arriving from the east had guiding centers at altitudes below GOES-10. This resulted in a lower GOES-10 fluence at times because these particles must have reached the vehicle via more complex trajectories with mirror points below GEO. Even at 20 MeV, where the proton gyroradius at GEO is approximately 1 Earth radius, the effective radial gradient of solar particles was sufficiently large to lower the integrated fluence measured at GOES-10.

[76] We have not used differential intensities from GOES satellites greater than the 80 to 200 MeV channel (which we plot at ~120 MeV). We find that solar proton data in the 200 to 1000 MeV range from the GOES satellites are difficult to reconcile with a smooth extrapolation of the spectra observed below 100 MeV. We have also made use of He intensities from the same web site in five channels that span the range from 4 to 500 MeV (1 to 125 MeV/nucleon).

[77] **Acknowledgments.** This work was supported by NASA under grants NNG04GB55G, NNG04088G, and NAG5-12929. We appreciate discussions with E. C. Stone, G. Li, R. Kallenbach, and G. P. Zank about particle transport and discussions with A. Vourlidas and N. Gopalswamy about CME kinetic energy estimates. We are also very grateful for the availability of GOES-11 data from NOAA's Space Environment Center at http://www.sec.noaa.gov/Data/index.html.

[78] Arthur Richmond thanks Gang Li and another reviewer for their assistance in evaluating this paper.

References

Bamert, K., et al. (2004), Hydromagnetic wave excitation upstream of an interplanetary traveling shock, *Astrophys. J.*, *601*, L99–L102.

Band, D., et al. (1993), BATSE observations of gamma-ray burst spectra. I. Spectral diversity, *Astrophys. J.*, *413*, 281–292.

Cane, H. V., T. T. von Rosenvinge, C. M. S. Cohen, and R. A. Mewaldt (2003), Two components in major solar particle events, *Geophys. Res. Lett.*, *30*(12), 8017, doi:10.1029/2002GL016580.

Cohen, C. M. S., et al. (1999), New observations of heavy-ion-rich solar particle events from ACE, *Geophys. Res. Lett.*, *26*, 2697.

Cohen, C. M. S., et al. (2005), Heavy ion abundances and spectra from the large SEP events of October–November 2003, *J. Geophys. Res.*, *110*, A09S16, doi:10.1029/2005JA011004.

Compton, A. H., and I. A. Getting (1935), An apparent effect of galactic rotation on the intensity of cosmic rays, *Phys. Rev.*, *47*, 817–821.

Cook, W. R., et al. (1993), PET: A Proton/Electron Telescope for studies of magnetospheric, solar, and galactic particles, *IEEE Trans. Geosci. Remote Sens.*, *31*, 5.

Droege, W. (1994), Transport of solar energetic particles, *Astrophys. J. Suppl. Ser.*, *90*, 567–576.

Ellison, D. C., and R. Ramaty (1985), Shock acceleration of electrons and ions in solar flares, *Astrophys. J.*, *298*, 400–408.

Emslie, A. G., et al. (2004), Energy partition in two solar flare/CME events, *J. Geophys. Res.*, *109*, A10104, doi:10.1029/2004JA010571.

Geiss, J. (1998), Constraints on the FIP mechanisms from solar wind abundance data, *Space Sci. Rev.*, *85*, 241–252.

Gold, R. E., et al. (1998), Electron, Proton, and Alpha Monitor on the Advanced Composition Explorer spacecraft, *Space Sci. Rev.*, *86*, 541.

Gopalswamy, N., et al. (2005), Coronal mass ejections during the violent solar eruptions of 2003 October and November, *J. Geophys. Res.*, *110*, A09S15, doi:10.1029/2004JA010958.

Grevesse, N., and A. J. Sauval (1998), Standard solar composition, *Space Sci. Rev.*, *85*, 161–174.

Haggerty, D. K., E. C. Roelof, G. C. Ho, and R. E. Gold (2005), Qualitative comparison of ACE/EPAM from different detector heads: Implications for NOAA RTSW users, *Adv. Space Res.*, in press.

Hurford, G. J., R. A. Mewaldt, E. C. Stone, and R. E. Vogt (1975), Enrichment of heavy nuclei in ^{3}He-rich flares, *Astrophys. J.*, *201*, L95–L97.

Kallenbach, R., K. Bamert, M. Hilchenbach, and C. W. Smith (2005), Observations of turbulence near interplanetary shocks, in *Physics of Collisionless Shocks, Proceedings of the 4th International IGPP Conference*, *AIP Conf. Proc.*, edited by G. Li et al., in press.

Laming, J. M., and U. Feldman (2001), The solar helium abundance in the outer corona determined from observations with SUMER/SOHO, *Astrophys. J.*, *546*, 552–558.

Lee, M. A. (1983), Coupled hydrodynamic wave excitation and ion acceleration at interplanetary traveling shocks, *J. Geophys. Res.*, *88*, 6109–6119.

Li, G., and G. P. Zank (2005), Mixed particle acceleration at CME-driven shocks and flares, *Geophys. Res. Lett.*, *32*, L02101, doi:10.1029/2004GL021250.

Li, G., G. P. Zank, and W. K. M. Rice (2005), Acceleration and transport of heavy ions at coronal mass ejection-driven shocks, *J. Geophys. Res.*, *110*, A06104, doi:10.1029/2004JA010600.

Lin, R. P. (1985), Energetic solar electrons in the interplanetary medium, *Sol. Phys.*, *100*, 537–561.

Lin, R. P., R. A. Mewaldt, and M. A. I. Van Hollebeke (1982), The energy spectrum of 20 keV–20 MeV electrons accelerated in large solar flares, *Astrophys. J.*, *253*, 949–962.

Lodders, K. (2003), Solar system abundances and condensation temperatures of the elements, *Astrophys. J.*, *591*, 1220–1247.

Looper, M. D., J. B. Blake, J. R. Cummings, and R. A. Mewaldt (1996), SAMPEX observations of energetic hydrogen isotopes in the inner zone, *Radiat. Measure.*, *26*(6), 967–978.

Mason, G. M., et al. (1998), The Ultra Low Energy Isotope Spectrometer (ULEIS) for the ACE spacecraft, *Space Sci. Rev.*, *86*, 409–448.

Mason, G. M., et al. (1999a), Particle acceleration and sources in the November 1997 solar energetic particle events, *Geophys. Res. Lett.*, *26*, 141–144.

Mason, G. M., J. E. Mazur, and J. R. Dwyer (1999b), ^{3}He enhancements in large solar energetic particle events, *Astrophys. J. Lett.*, *525*, L133–L136.

Mason, G. M., et al. (2002), Spectral properties of He and heavy ions in ^{3}He-rich solar flares, *Astrophys. J.*, *574*, 1039–1058.

Mazur, J. E., G. M. Mason, B. Klecker, and R. E. McGuire (1992), The energy spectra of solar flare hydrogen, helium, oxygen, and iron: Evidence for stochastic acceleration, *Astrophys. J.*, *401*, 398–410.

Mazur, J. E., G. M. Mason, B. Klecker, and R. E. McGuire (1993), The abundances of hydrogen, helium, oxygen, and iron accelerated in large solar particle events, *Astrophys. J.*, *404*, 810–817.

Mewaldt, R. A., et al. (2001), Long-term fluences of energetic particles in the heliosphere, in *Solar and Galactic Composition*, *AIP Conf. Proc.*, *598*, 165–170.

Mewaldt, R. A., et al. (2003), Impulsive flare material: A seed population for large solar particle events?, *Proc. Int. Cosmic Ray Conf. 26th*, *6*, 3313–3316.

Mewaldt, R. A., et al. (2005), Solar energetic particle spectral breaks, in *Physics of Collisionless Shocks, Proceedings of the 4th International IGPP Conference*, *AIP Conf. Proc.*, edited by G. Li et al., 227–232.

Moses, D., W. Droege, P. Meyer, and P. Evenson (1989), Characteristics of energetic solar flare electron spectra, *Astrophys. J.*, *346*, 523–530.

Ng, C. K., D. V. Reames, and A. J. Tylka (2003), Modeling shock-accelerated solar energetic particles coupled to interplanetary Alfven waves, *Astrophys. J.*, *591*, 461–485.

Onsager, T. G., et al. (1996), Operational uses of the GOES energetic particle detectors, in *GOES-8 and Beyond*, edited by E. R. Washwell, *SPIE Conf. Proc.*, *2812*, 281–290.

Reames, D. V. (1995), Coronal abundances determined from energetic particles, *Adv. Space Res.*, *15*(7), 41–51.

Reames, D. V. (1999), Particle acceleration at the sun and in the heliosphere, *Space Sci. Rev.*, *90*, 413.

Reames, D. V., S. W. Kahler, and C. K. Ng (1997), Spatial and temporal invariance in the spectra of energetic particles in gradual solar flares, *Astrophys. J.*, *491*, 414–420.

Skoug, R. M., J. T. Gosling, J. T. Steinberg, D. J. McComas, C. W. Smith, N. F. Ness, Q. Hu, and L. F. Burlaga (2004), Extremely high speed solar wind: 29–30 October 2003, *J. Geophys. Res.*, *109*, A09102, doi:10.1029/2004JA010494.

Smith, C. W., et al. (2001), ACE observations of the Bastille Day 2000 interplanetary disturbances, *Sol. Phys.*, *204*, 227–252.

Stone, E. C., et al. (1998a), The Solar Isotope Spectrometer for the Advanced Composition Explorer, *Space Sci. Rev.*, *86*, 357–408.

Stone, E. C., et al. (1998b), The Advanced Composition Explorer, *Space Sci. Rev.*, *86*, 1–22.

Tylka, A. J., P. R. Boberg, R. E. McGuire, C. K. Ng, and D. V. Reames (2000), Temporal evolution in the spectra of gradual solar energetic particle events, in *Acceleration and Transport of Energetic Particles Observed in the Heliosphere*, edited by R. A. Mewaldt et al., *AIP Conf. Proc.*, *528*, 147–152.

Tylka, A. J., et al. (2001), Evidence for remnant flare suprathermals in the source population of solar energetic particles in the 2000 Bastille Day event, *Astrophys. J.*, *558*, L59–L63.

Tylka, A. J., et al. (2005), Shock geometry, seed populations, and the origin of variable elemental composition at high energies in large gradual solar particle events, *Astrophys. J.*, *625*, 474–495.

Turner, R. (1995), Risk management strategies during solar particle events on a human mission to Mars or the Moon, report, ANSER, Arlington, Va.

von Steiger, R., J. Geiss, and G. Gloeckler (1998), Composition of the solar wind, in *Cosmic Winds and the Heliosphere*, edited by J. R. Jokipii, C. P. Sonett, and M. S. Giampapa, pp. 581–616, Univ. of Ariz. Press, Tucson.

von Steiger, R., et al. (2000), Composition of quasi-stationary solar wind flows from Ulysses/Solar Wind Ion Composition Spectrometer, *J. Geophys. Res.*, *105*, 27,217–27,238.

Wiedenbeck, M. E., et al. (2000), Enhanced abundances of ^{3}He in large solar energetic particle events, in *Acceleration and Transport of Energetic Particles Observed in the Heliosphere*, edited by R. A. Mewaldt et al., *AIP Conf. Proc.*, *528*, 131–134.

Yanasak, N. E., et al. (2001), Measurement of the secondary radionuclides of ^{10}Be, ^{26}Al, ^{36}Cl, ^{54}Mn, and ^{14}C, and implications for the galactic cosmic-ray age, *Astrophys. J.*, *563*, 768–792.

Zank, G. P., W. K. M. Rice, and C. C. Wu (2000), Particle acceleration and coronal mass ejection driven shocks: A theoretical model, *J. Geophys. Res.*, *105*, 25,079–25,095.

C. M. S. Cohen, A. W. Labrador, R. A. Leske, and R. A. Mewaldt, MC 220-47, California Institute of Technology, Pasadena, CA 91125, USA. (cohen@srl.caltech.edu; labrador@srl.caltech.edu; ral@srl.caltech.edu; rmewaldt@srl.caltech.edu)

M. I. Desai and G. M. Mason, University of Maryland, College Park, MD 20742, USA. (desai@uleis.umd.edu; gmmason@umd.edu)

D. K. Haggerty, Johns Hopkins University Applied Physics Laboratory, Laurel, MD 20723, USA. (dennis.haggerty@jhuapl.edu)

M. D. Looper, J. E. Mazur, and R. S. Selesnick, The Aerospace Corporation, Los Angeles, CA 90009, USA. (mark.d.looper@aero.org; joseph.e.mazur@aero.org; richard.s.selesnick@aero.org)

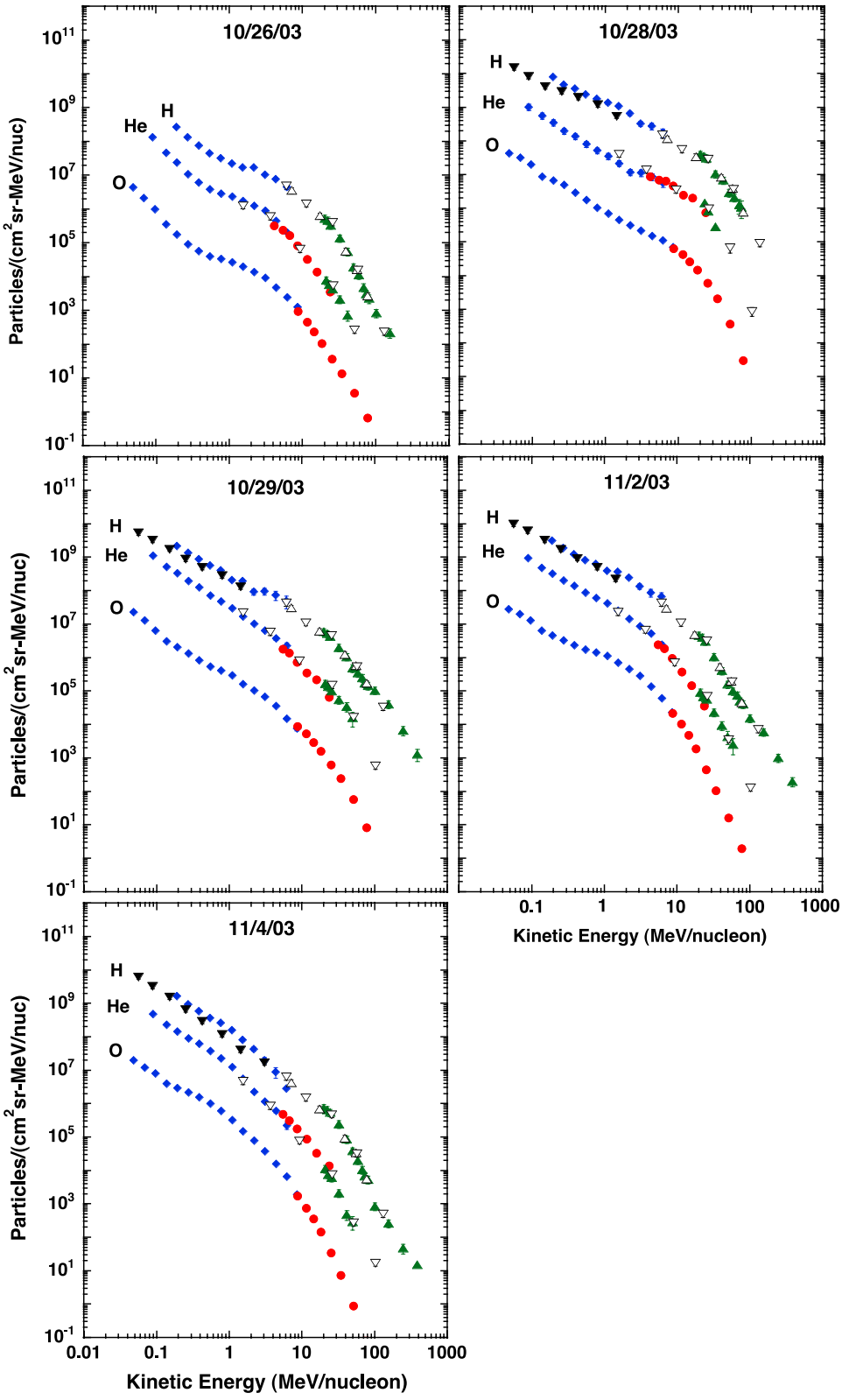

Figure 2. Integrated fluence spectra of H, He, and O for the five SEP events in this study. The data are from ULEIS (filled diamonds), EPAM (downward filled triangles), SIS (filled circles), PET (filled upward triangles), and GOES-11 (upward and downward open triangles).